Mid-Holocene European climate revisited: New high-resolution regional climate model simulations using pollen-based land-cover

Gustav Strandberg, Johan Lindström, Anneli Poska, Qiong Zhang, Ralph Fyfe, Esther Githumbi, Erik Kjellström, Florence Mazier, Anne Nielsen, Shinya Sugita, et al.

Quaternary Science Reviews 281 (2022) 107431

Contents lists available at ScienceDirect

Quaternary Science Reviews

journal homepage: www.elsevier.com/locate/quascirev

Mid-Holocene European climate revisited: New high-resolution regional climate model simulations using pollen-based land-cover

Gustav Strandberg [a, b, *], Johan Lindström [c], Anneli Poska [d, h], Qiong Zhang [b, e], Ralph Fyfe [f], Esther Githumbi [g, h], Erik Kjellström [a, b], Florenze Mazier [i], Anne Birgitte Nielsen [j], Shinya Sugita [k], Anna-Kari Trondman [g, l], Jessie Woodbridge [f], Marie-José Gaillard [g]

[a] Rossby Centre, Swedish Meteorological and Hydrological Institute, SMHI, Norrköping, SE-602 19, Sweden
[b] Bolin Centre for Climate Research, Stockholm University, Stockholm, SE-106 91, Sweden
[c] Centre for Mathematical Sciences, Lund University, SE-221 00, Lund, Sweden
[d] Department of Geology, Tallinn University of Technology, 19086, Tallinn, Estonia
[e] Department of Physical Geography, Stockholm University, Stockholm, SE-106 91, Sweden
[f] School of Geography, Earth and Environmental Sciences, University of Plymouth, Plymouth, PL4 8AA, UK
[g] Department of Biology and Environmental Science, Linnaeus University, SE-39231, Kalmar, Sweden
[h] Department of Physical Geography and Ecosystem Science, Lund University, SE-221 00, Sweden
[i] Department of Environmental Geography, UMR-CNRS 5602, Toulouse Jean Jaurès University, Toulouse, C229, France
[j] Department of Geology, Lund University, SE-221 00, Sweden
[k] Institute of Ecology, Tallinn University, Tallinn, Estonia
[l] Division of Educational Affairs, Swedish University of Agricultural Sciences, Lomma, SE-234 22, Sweden

ARTICLE INFO

Article history:
Received 9 November 2021
Received in revised form
24 January 2022
Accepted 16 February 2022
Available online xxx

Handling Editor: Donatella Magri

Keywords:
Paleoclimate
Global climate model
Dynamical vegetation model
Vegetation reconstruction
Spatial statistical models
Land-use and land-cover change
REVEALS
LPJ-GUESS
EC-Earth
RCA4
HCLIM

ABSTRACT

Land-cover changes have a clear impact on local climates via biophysical effects. European land cover has been affected by human activities for at least 6000 years, but possibly longer. It is thus highly probable that humans altered climate before the industrial revolution (AD1750–1850). In this study, climate and vegetation 6000 years (6 ka) ago is investigated using one global climate model, two regional climate models, one dynamical vegetation model, pollen-based reconstruction of past vegetation cover using a model of the pollen-vegetation relationship and a statistical model for spatial interpolation of the reconstructed land cover. This approach enables us to study 6 ka climate with potential natural and reconstructed land cover, and to determine how differences in land cover impact upon simulated climate. The use of two regional climate models enables us to discuss the robustness of the results. This is the first experiment with two regional climate models of simulated palaeo-climate based on regional climate models.

Different estimates of 6 ka vegetation are constructed: simulated potential vegetation and reconstructed vegetation. Potential vegetation is the natural climate-induced vegetation as simulated by a dynamical vegetation model driven by climate conditions from a climate model. Bayesian spatial model interpolated point estimates of pollen-based plant abundances combined with estimates of climate-induced potential un-vegetated land cover were used for reconstructed vegetation. The simulated potential vegetation is heavily dominated by forests: evergreen coniferous forests dominate in northern and eastern Europe, while deciduous broadleaved forests dominate central and western Europe. In contrast, the reconstructed vegetation cover has a large component of open land in most of Europe.

The simulated 6 ka climate using reconstructed vegetation was 0–5 °C warmer than the pre-industrial (PI) climate, depending on season and region. The largest differences are seen in north-eastern Europe in winter with about 4–6 °C, and the smallest differences (close to zero) in southwestern Europe in winter. The simulated 6 ka climate had 10–20% more precipitation than PI climate in northern Europe and 10–20% less precipitation in southern Europe in summer. The results are in reasonable agreement with proxy-based climate reconstructions and previous similar climate modelling studies. As expected, the global model and regional models indicate relatively similar climates albeit with regional differences indicating that, models response to land-cover changes differently.

* Corresponding author. Rossby Centre, Swedish Meteorological and Hydrological Institute, SMHI, Norrköping, SE-602 19, Sweden.
E-mail address: gustav.strandberg@smhi.se (G. Strandberg).

https://doi.org/10.1016/j.quascirev.2022.107431

The results indicate that the anthropogenic land-cover changes, as given by the reconstructed vegetation, in this study are large enough to have a significant impact on climate. It is likely that anthropogenic impact on European climate via land-use change was already taking place at 6 ka. Our results suggest that anthropogenic land-cover changes at 6 ka lead to around 0.5 °C warmer in southern Europe in summer due to biogeophysical forcing.

1. Introduction

Land-use and land-cover change (LULCC) as a means of climate-change mitigation has received an increasing interest in recent years (e.g. Smith et al., 2016a; Williamson, 2016; Griscom et al., 2017). Emissions scenarios compliant with the goal of the Paris Agreement to limit global warming to "well below 2°C" (UNFCCC, 2010; UNFCCC, 2015) are partly reliant upon different ways to achieve carbon uptake, capture and sequestration (IPCC, 2018). Meeting these targets implies that LULCC will need to change drastically at the global scale over the coming decades. In theory, afforestation as mitigation measure could limit global warming because increased biomass would decrease the amount of carbon dioxide (CO_2) in the atmosphere via biogeochemical processes, primarily carbon fixation by plants via photosynthesis. Further, bioenergy with carbon capture and storage (BECCs) has become to be considered as one of the most realistic and cost-effective technologies for negative emissions as it combines the use of biomass with geological storage of CO_2. However, changes in land-cover also have biogeophysical effects affecting the albedo, surface roughness and heat fluxes (e.g. plant evapotranspiration), which in turn will influence regional climate and may limit the positive effect of a wide-spread application of such mitigation measures (e.g. Smith et al., 2016a). The biogeophysical effects have been less studied than the biogeochemical ones. However, several studies have shown that regional climatic responses to LULCC can differ depending on the season and the geographical location (e.g. Jia et al., 2019; Strandberg and Kjellström, 2019). Thus, the overall positive global effects of land cover-based mitigation strategies may have negative regional effects.

Henceforth, we use the term LULCC primarily to describe deforestation by humans, i.e. replacement of tree vegetation by low vegetation (herbs and low shrubs), although past land-use changes have had other consequences on land cover, such as transformation of grazing and cultivated land into woodland due to shifting cultivation or land abandonment. LULCC is thus synonym of "anthropogenic land-cover change" (ALCC) (e.g. Kaplan et al., 2009), a term also commonly used in the literature. The identification of the most suitable climate-change mitigation strategies still requires a better understanding of the biogeophysical effects of LULCC on climate, and a better estimate of the net effects (biogeophysical and − chemical). This can be achieved with idealized climate model simulations, e.g. evaluating the effect of complete afforestation or deforestation of a large area of the globe such as a continent (e.g. Boysen et al., 2020; Davin et al., 2020). It can also be studied with palaeoclimate model simulations using reconstructions of past LULCC over long time periods, and either Global Climate Models (GCMs) (He et al., 2014; Smith et al., 2016b; Gilgen et al., 2019) or regional climate models (RCMs) (Strandberg et al., 2014; Russo and Cubash, 2016; Velasquez et al., 2021). Such studies have the advantage to investigate the effects of realistic LULCC on past climate, and climate-model simulations can be evaluated with palaeoclimate proxies. However, such studies are few; moreover, it has also been argued that the study of LULCC as a climate forcing requires the use of high-resolution RCMs to better account for the biogeophysical forcing of LULCC that operates at a regional scale rather than at a global scale (e.g. Gaillard et al., 2010; Strandberg et al., 2014). The higher density of the horizontal grid spacing in RCMs (usually 10–50 km) than in GCMs (usually 100–200 km) (e.g. Rummukainen, 2016) is also an advantage in palaeoclimate modelling if the model output is to be compared with proxy data that generally represent local scale climate (Ludwig et al., 2018, 2019; Giorgi, 2019). Only two such studies using RCMs exist for Europe (Strandberg et al., 2014; Russo and Cubasch, 2016). These studies were first attempts at evaluating the potential of RCMs to study climate conditions during the Holocene at the European scale. They provided new insights on temperature difference (Strandberg et al., 2014) and temperature changes (Russo and Cubash, 2016; Russo et al., 2021) between 6000 years BP (henceforth 6 ka; Mid Holocene conditions) and 1750 CE (200 years BP, henceforth 0.2 ka). Strandberg et al. (2014) also investigated the effect of LULCC at 6 ka and 0.2 ka. Both studies demonstrated the need for more RCM studies of Holocene climate to better understand past climate change and climate forcings at a regional scale, and in particular further elucidate the regional effect of LULCC in Europe.

In this study, we revisit the climate in Europe at 6 ka (representing Mid Holocene and the "Neolithic Revolution") and 1850, a pre-industrial time slice commonly used to represent a base line for the most recent climate that is little influenced by human activities (henceforth PI). The objective is to investigate the sensitivity of regional climate models (RCMs) (in terms of simulated climate) to the first substantial LULCC in Europe related to the "Neolithic revolution", i.e. the introduction of crop cultivation and cattle grazing (e.g. Bocquet-Appel, 2011), in comparison with no LULCC (i.e. climate-induced, natural vegetation, also termed "potential vegetation"). The 6 ka climate (with and without LULCC) is then compared with PI climate; a recent period that is still not that affected by anthropogenic greenhouse gas emissions. The major differences between this new study and that of Strandberg et al. (2014) are (a) the use of two RCM models instead of one and (b) pollen-based LULCC reconstructions as land-use forcing, rather than LULCC scenarios such as the commonly used KK10 (Kaplan et al., 2009) or HYDE (Klein Goldewijk et al., 2017) scenarios. The latter are largely based on population growth models and hypotheses. It is the first time that the use of more realistic LULCC reconstructions (based on empirical pollen data) is tested at the scale of Europe. We use the latest pollen-based REVEALS land-cover reconstruction for Europe (Githumbi et al., 2021), i.e. an extension of the reconstruction by Trondman et al. (2015) both in terms of number of pollen records used and spatial coverage. It is a gridded reconstruction with a spatial scale of one degree. REVEALS is a model of the pollen-vegetation relationship integrating models of dispersion of small particles in the air and their deposition (Sugita, 2007). Such pollen-based REVEALS datasets of past land cover have not been used in climate modelling thus far, although these reconstructions now exist for over most of the northern hemisphere (e.g. Dawson et al., 2018). Because of the gaps in the spatial

distribution of pollen records, the gridded REVEALS reconstruction is interpolated into a continuous gridded land-cover dataset for its use in RCM simulations. This is achieved with spatial statistical models (e.g. Pirzamanbein et al., 2014, 2020). Potential vegetation, i.e. land cover without LULCC, is simulated by a dynamic vegetation model (DVM).

Comparison between 6 ka and PI climates at the regional scale has also an interest within the 'Holocene temperature conundrum' (HTC) debate (e.g. Liu et al., 2014; Bader et al., 2020). HTC refers to the disagreement between the Holocene expected global warming due to increasing greenhouse gases and retreating ice sheets as simulated by global climate models, and the Holocene cooling shown by the first global palaeoecological reconstruction of Holocene climate (Marcott et al., 2013). Among the explanations of the HTC, both deficiencies in climate models and in the analysis of climate-model outputs, as well as biases in the palaeoecological global reconstruction have been proposed (e.g. Liu et al., 2014). Both HTC and regional data-model inconsistencies have also been hypothesised to be partly a consequence of not adequately accounting for LULCC from c. 6 ka in Europe (e.g. Kaplan et al., 2010; Ruddiman et al., 2015; Stocker et al., 2017; Harrison et al., 2018, 2020). In this paper, we also revisit this question in the light of our results.

2. Models and data

2.1. Model chain

This study builds upon a chain of model simulations (see detailed model descriptions below). Within the first step, 6 ka and pre-industrial (1850 CE, hereafter PI) climate conditions are simulated by the GCM EC-Earth using present day vegetation (Fig. 1 and Table 1). These climate conditions are then used to force the RCMs RCA4 and HCLIM over the European domain; thus, simulating the climate at the same periods as the GCM, but at higher horizontal resolution and with their own physical parameterisations. For each RCM, the model output includes a high-resolution climate simulation for 6 ka and PI respectively (6k-0 and PI in Table 1). The two representations of 6 ka climate, as simulated by the RCMs, are used to force the DVM LPJ-GUESS to estimate a potential vegetation cover consistent with each simulated climate. Under 6 ka climate condition, two simulated potential vegetation cover reconstructions are estimated, one based on EC-Earth + RCA4 + LPJ-GUESS (L1 in Table 1) driven by climate simulated by RCA4 and one based on EC-Earth + HCLIM + LPJ-GUESS (L2 in Fig, 1 and Table 1) driven by climate simulated by HCLIM. In this context, 'potential' refers to vegetation that is allowed to grow freely without human intervention, i.e. it is the natural climate-induced vegetation as simulated by the DVM. These two vegetation covers are then fed back to both RCA4 and HCLIM to simulate 6 ka climate with vegetation cover consistent with simulated mid-Holocene climate (6k-L1 when land cover L1 is used and 6k-L2 when L2 is used). PI vegetation is assumed to be the same as the present vegetation, and is not simulated by LPJ-GUESS.

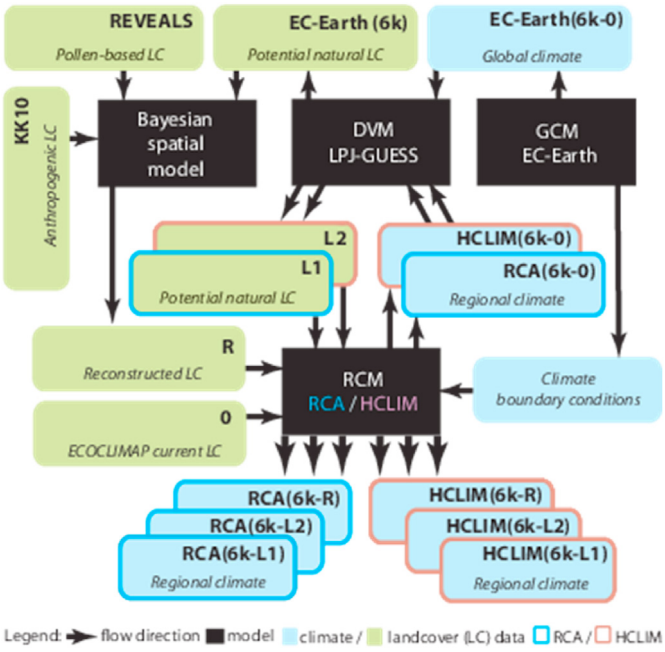

Fig. 1. Description of the model chain for 6 ka. All RCM simulations read boundary conditions from EC-Earth. A first set of simulations are made with current land cover (0), these climate scenarios are used in LPJ-GUESS to provide the 6 ka potential natural land cover (L1, L2) subsequently used in the RCMs. A Bayesian spatial model is used to reconstruct 6 ka land cover (R) that is also used in the RCMs.

In parallel, the 6 ka vegetation is reconstructed at a 1° spatial scale using multiple pollen records and the REVEALS model (Sugita, 2007; Githumbi et al., 2021). Proxy-based vegetation cover is not available for all 1° grid cells due to the irregular distribution of pollen records. Therefore, pollen-based vegetation cover is interpolated over the entire grid covering Europe using spatial statistics (Pirzamanbein et al., 2018) and additional co-variates including simulated vegetation from LPJ-GUESS (driven by the EC-Earth simulation) and the KK10 anthropogenic land-cover scenario for 6 ka (Kaplan et al., 2009). This reconstruction (6k-R in Fig. 1 and Table 1) represents the "actual" 6 ka vegetation, i.e. a combination of climate-induced potential vegetation and human-induced vegetation.

The benefit of this approach compared to coupled simulations is that it is possible to carry out sensitivity tests using different vegetation cover estimates in otherwise similar simulations. This allows us to study the effect of vegetation on climate, and how this effect is simulated in different RCMs. It also allows a multi-model estimate of 6 ka vegetation and climate to be produced.

2.2. EC-Earth3-LR

The lateral boundary conditions for the RCMs are taken from simulations with the fully coupled general circulation model EC-Earth version 3.1 (Hazeleger et al., 2010) with active atmosphere (IFS), land (H-TESSEL), ocean (NEMO3.6), and sea-ice (LIM3) components. The atmospheric component has T159 horizontal spectral resolution (approximately 1.125° × 1.125°) with 62 vertical levels. The Ocean model NEMO (Madec, 2008) has a horizontal resolution of approximately 1° × 1° and 46 vertical levels. The ocean surface part is coupled with the sea-ice model LIM3 (Vancoppenolle et al., 2009). The atmospheric (IFS) and oceanic models (NEMO-LIM) are coupled through the coupler OASIS3 (Valcke, 2013) every 3 h. In past years, the EC-Earth3-LR has been used to study the mid-Holocene climate change e.g. the climate response to a greening of Sahara (Muschitiello et al., 2015; Pausata et al., 2016; Lu et al., 2018).

The PI (1850 CE) and 6 ka simulations are performed following the PMIP4 protocol (Otto-Bliesner et al., 2017). For the 6 ka simulation, the changes in climate forcing are orbital parameters and CO_2 and methane concentration. The orbital forcing is calculated in the model according to Berger (1978) for PI and 6 ka. The CO_2 concentration is 284.7 ppm_v for PI and 264.4 ppm_v for 6 ka, and methane concentration is 760 ppb_v for PI and 650 ppb_v for PI. All other climate forcing factors (i.e. aerosols) and boundary conditions

Table 1
The combination of models and land cover (LC) used in each simulation. The DVM is driven by climate conditions from RCA4 (6k-0) and HCLIM(6k-0) which yields the new LCs L1 and L2 respectively; these are then used in subsequent climate simulations.

Simulation	Time	GCM	RCM	LC	DVM	New LC
RCA (PI)	PI	EC-Earth3-LR	RCA4	Current veg.		
HCLIM(PI)	PI	EC-Earth3-LR	HCLIM	Current veg.		
RCA (6k-0)	6 ka	EC-Earth3-LR	RCA4	Current veg.		
					LPJ-GUESS	→L1
HCLIM(6k-0)	6 ka	EC-Earth3-LR	HCLIM	Current veg.		
					LPJ-GUESS	→L2
RCA (6k-L1)	6 ka	EC-Earth3-LR	RCA4	L1		
RCA (6k-L2)	6 ka	EC-Earth3-LR	RCA4	L2		
HCLIM(6k-L1)	6 ka	EC-Earth3-LR	HCLIM	L1		
HCLIM(6k-L2)	6 ka	EC-Earth3-LR	HCLIM	L2		
RCA (6k-R)	6 ka	EC-Earth3-LR	RCA4	Reconstruction		
HCLIM(6k-R)	6 ka	EC-Earth3-LR	HCLIM	Reconstruction		

(i.e. land-sea mask, orography) are the same in PI and 6 ka. The vegetation cover used in PI and 6k-0 simulations was prescribed based on modern satellite observations (ECMWF, 2009). The model setup for PI and 6 ka with EC-Earth3-LR is the same as the PMIP4 simulations as described in Zhang et al. (2021). The 6 ka simulation is run for a 500 year period, the initial conditions are from a 700-year PI spin-up run. The climate quasi-equilibrium (defined as a global mean surface temperature trend of less than 0.05 °C per century and a stable Atlantic meridional overturning circulation (Kageyama et al., 2018)) is reached after 200 years and we use 6-hourly data as the lateral boundary condition for the RCMs.

2.3. RCA4 and HCLIM

The use of regional climate models (RCM) adds geographical details and improves the simulation of climatic processes as the horizontal grid spacing is denser in RCMs (usually 10–50 km) than in GCMs (usually 100–200 km) (e.g. Rummukainen, 2016). The Rossby Centre Atmosphere model (RCA4, Strandberg et al., 2015; Kjellström et al., 2016) has been widely used for modelling future climate; mainly over Europe, but also for many other parts of the world (e.g. Dosio et al., 2020; Rana et al., 2020). RCA3, the predecessor of RCA4, has also been used in studies of palaeoclimate (MIS 3, Kjellström et al., 2010; LGM, Strandberg et al., 2011; 6 ka, Strandberg et al., 2014; the last millennium, Schimanke et al., 2012). Here, RCA4 is run with 24 vertical levels and a time step of 20 min, made possible by semi-Lagrangian discretisation (Källén, 1996). Radiation is parameterised with the Savijärvi Hirlam radiation scheme (Savijärvi, 1990), turbulence with the CBR turbulent kinetic energy based scheme (Marquet, 2008), condensation and convection with the Bechtold-KF scheme (Bechtold et al., 2001). Land surface processes are parameterised with the RCA land-surface scheme (Samuelsson et al., 2006).

The HCLIM38-ALADIN (HCLIM, Belušić et al., 2020) has been used in future climate simulations for European, African and Arctic domains (Belušić et al., 2020; Lind et al., 2020). HCLIM is run with 65 vertical levels and a time step of 20 min, made possible by a semi Lagrangian scheme (Ritchie et al., 1995; Robert et al., 1972; Simmons et al., 1978; Temperton et al., 2001). Convection is parameterised with KFB (Bechtold et al., 2001; Bazile et al., 2012), micro-physics from Lopez (2002) and Bouteloup et al. (2005), turbulence with CBR (Cuxart et al., 2000), land surface processes with SURFEX (Masson et al., 2013) and radiation with RRTM_LW, SW6 (Mlawer et al., 1997; Iacono et al., 2008; Fouquart and Bonnel, 1980).

Both RCMs are run on a horizontal grid spacing of 0.44° (corresponding to approximately 50 km) across Europe (the CORDEX EUR-44 domain (Jacob et al., 2014)). Every 6 h, the RCMs read humidity, temperature, wind and surface pressure from EC-Earth3-LR along the lateral boundaries of the model domain, and sea surface temperature and sea ice extent within the model domain. Changing orbital forcing is not an option in the current versions of the RCMs used here. The solar constant and amount of greenhouse gases are maintained at pre-industrial levels in all experiments. The RCMs should nevertheless be able to reproduce 6 ka climate as the climate to a large degree is governed by the GCM (Kjellström et al., 2018; Vautard et al., 2020; Strandberg and Lind, 2021) even with different insolation (Kjellström et al., 2010). For PI, a simulation of 30 years is analysed, for 6 ka a 50 year period. We calculate the average of the nominal season's winter (December, January and February; henceforth DJF) and summer (June, July and August; henceforth JJA).

2.4. LPJ-GUESS

The dynamic vegetation model (DVM) LPJ-GUESS (Lund-Potsdam-Jena General Ecosystem Simulator) used in this study is an individual-based ecosystem model optimized for regional studies (Smith et al., 2001, 2014; Sitch et al., 2003). Model performance in terms of reproducing vegetation, hydrological and biogeochemical cycles for past applications has been tested in several studies (Miller et al., 2008; Garreta et al., 2010; Lu et al., 2018). The model has been repeatedly applied and benchmarked for European conditions (Miller et al., 2008; Hickler et al., 2012). LPJ-GUESS has been run together with RCA3 for different time periods (Kjellström et al., 2010; Strandberg et al., 2011, 2014).

In order to simulate potential natural vegetation cover for Europe at 6 ka, LPJ-GUESS used the climate input scenarios from the GCM and RCMs described above. LPJ-GUESS reads temperature, precipitation (amount and number of days) and radiation (in- and outgoing short- and longwave) from the climate models. The spatial resolution of the simulations was inherited from the climate inputs. The CO_2 level was set to 265 ppm (Augustin et al., 2010), which is almost the same concentration as the forcing set in EC-Earth3-LR 6 ka simulation. In order to reach a stable vegetation composition, a spin-up period of 300 years was implemented using the first 10 years of the simulation in a randomized way. A set of plant functional types (PFTs) based on major European tree species was applied (Hickler et al., 2012). Vegetation cover fractions were calculated based on the averaged output of PFT specific leaf area index (LAI) over the last 30 years of the simulation period. The LAI was converted into fractional plant cover (FPC) using a simplified version of the Lambert-Beer's law: $FPC=(1.0-\exp(-0.5*LAI_{PFT}))$ (Monsi and Saeki, 1953; Prentice et al., 1993). The vegetation input

for the RCMs was generated by summing the FPCs of the simulated PFTs into three land-cover types: summer-green trees (ST), evergreen trees (ET) and open land (OL) (Table 2). The fraction of non-vegetated area was estimated by subtracting summed vegetation cover from one. For usage as co-variate in the spatial interpolation model, the vegetation cover fractions were proportionally reduced by the anthropogenic land-cover deforestation estimate at 6 ka derived from the ALCC model KK10 (Kaplan et al., 2011).

2.5. REVEALS

REVEALS (Regional Estimates of Vegetation Abundance from Large Sites) is a model that was developed to estimate regional vegetation cover at a scale of 10^4–10^5 km^2 using pollen records from large lakes (100–500 ha) (Sugita, 2007). REVEALS requires dates, records of pollen counts, relative pollen productivities of plants, values of fall speed of pollen, and a model of pollen dispersal and deposition. The output is plant percentage cover with an associated standard error. The REVEALS model can also be applied on pollen records from multiple small sites (lakes and bogs), the standard error will however be larger than with pollen data from large lakes (Sugita, 2007; Trondman et al., 2015, 2016). For use in climate modelling, REVEALS estimates of plant cover are achieved at a 1° grid scale using all suitable (see below) pollen records available in each grid cell. A REVEALS land cover reconstruction was previously performed for a large part of Europe (Trondman et al., 2015). The requirements and criteria for pollen records to be suitable are listed in Trondman et al. (2015) as well as all details on the pollen data handling and parameter settings for the REVEALS application (Mazier et al., 2012; Trondman et al., 2015; Appendix S2: The LandClim protocol). For the purpose of this study, we increased the coverage of the REVEALS reconstruction southwards to the Mediterranean area and eastwards to western Russia and the Middle East, and incorporated pollen records from new sites across the entire study region. The dataset increased from 636 pollen records (Trondman et al., 2015) to 1138 pollen records (Githumbi et al., 2021).

2.6. Spatial statistics

The spatial statistics estimation (see Pirzamanbein et al. (2018) and Pirzamanbein et al. (2020) for a complete description) uses computer intensive statistical inference methods (Roberts and Stramer, 2002; Brooks et al., 2011) to interpolate REVEALS model outputs (i.e. gridded pollen-based land-cover at a 1° grid) to all grid cells; providing complete vegetation cover across Europe. The spatial interpolation is a modified generalized linear mixed model with spatially dependent residuals. It has three main components:

1) The vegetation cover is modelled as compositional data (Aitchison, 1986) using a Dirichlet distribution (the generalized part of the generalized linear mixed model). This ensures that the interpolated fractions of vegetation cover are between 0 and 1 and sum to 1; thus 2) Large-scale features in the interpolation are modelled by regressing the REVEALS outputs onto a set of

Table 2
Groups of land-cover types used in this study. Ericaceae*(MTSE): the pollen productivity used for Ericaceae pollen in the REVEALS reconstruction represents the mean pollen productivity of several species of which *Arbutus unedo, Erica arborea, E. cinerea* and *E. multiflora* are dominant. The genus *Calluna vulgaris* (heather, LSE) also belongs to the Ericaceae family but its pollen productivity has been estimated separately (Githumbi et al., 2021). Cerealia t.: all cereals except *Secale cereale* (rye) that is easily that is easily separated on the basis of pollen morphology and for which pollen productivity was estimated separately. Abbreviation: t = type. of land-cover types (LCTs) and Plant Functionnal Types (PFTs) used in this study. **The most recent plant taxonomy has merged the family Chenopodiaceae into the family Amaranthaceae, i.e. "new" Amaranthaceae = "former" Amaranthaceae + Chenopodiaceae. Pollen analysts have mostly used the name Chenopodiaceae for this pollen-morphological type, but it includes all species from the two former families, therefore the name Amaranthaceae/Chenopodiaceae.

Land-cover types (LCTs)	PFT	PFT definition	Plant taxa/Pollen-morphological types
Evergreen trees and shrubs (ET)	TBE1	Shade-tolerant evergreen trees	*Picea abies* (Norway spruce)
	TBE2	Shade-tolerant evergreen trees	*Abies alba* (Silver fir)
	IBE	Shade-intolerant evergreen trees	*Pinus sylvestris* (Scots pine)
	MTBE	Mediterranean shade-tolerant broadleaved evergreen trees	*Phillyrea* (mock privet)
			Pistacia (lentisk, mastic)
			Quercus evergreen t. (evergreen oak species)
	TSE	Tall shrub, evergreen	*Juniperus communis* (common juniper)
	MTSE	Mediterranean broadleaved tall shrubs, evergreen	Ericaceae* (heather family)
			Buxus sempervirens (common box)
Summer-green trees and shrubs (ST)	IBS	Shade-intolerant summer-green trees	*Alnus glutinosa* (common alder)
			Betula (birch species)
	TBS	Shade-tolerant summer-green trees	*Carpinus betulus* (common hornbeam)
			Carpinus orientalis (oriental hornbeam)
			Castanea sativa (sweet chestnut)
			Corylus avellana (common hazel)
			Fagus sylvatica (European beech)
			Fraxinus (ash species)
			Quercus deciduous t. (summer-green oak species)
			Tilia (linden species)
			Ulmus (elm species)
	TSD	Tall shrub, summer-green	*Salix* (willow species (osier, sallow))
Open land (OL)	LSE	Low shrub, broadleaved evergreen	*Calluna vulgaris* (heather)
	GL	Grassland - all herbs	*Artemisia* (mugwort species)
			Amaranthaceae/Chenopodiaceae (amaranth family/e.g. goosefoot**)
			Cyperaceae (sedges)
			Filipendula (meadowsweet)
			Poaceae (grass family)
			Plantago lanceolata (ribwort plantain)
			Rumex acetosa-t (common sorrel and some other *Rumex* (dock) species)
	AL	Agricultural land - cereals	Cerealia-t (all cereals except *Secale cereale* (rye))
			Secale cereale (rye)

covariates (the linear component). The covariates used here consist of elevation and potential vegetation from LPJ-GUESS, driven by the EC-Earth climate model, and adjusted for the KK10 anthropogenic land cover. The regression essentially computes correlations between REVEALS outputs and covariates and then scales the covariates according to the correlation. Thus, the regression uses the spatial patterns of the covariates, but **not** their absolute values. A sensitivity study (Pirzamanbein et al., 2020) showed that the interpolation is reasonably insensitive to different possible covariates. 3) The spatial mixed effect, modelled using a Gaussian Markov Random Field (Lindgren et al., 2011), captures any spatial patterns in the REVEALS outputs, which are not found in the covariates. The final interpolation is subsequently a statistically optimal combination of these spatial patterns and the covariate information.

The spatial model provides pollen-based estimates of vegetation cover, and only accounts for vegetated areas. The final *reconstructed land-cover* (R) is obtained by adjusting the output from the statistical model with the fraction of bare ground from LPJ-GUESS simulated potential natural vegetation using EC-Earth derived 6 ka climate data. This adjustment enhances land cover openness in sparsely vegetated areas, such as the OL (open land) fraction of the REVEALS-based vegetation reconstruction in grids with simulated bare ground, such as in mountainous regions in the Alps and northern Scandinavia and along northern coasts.

3. Results

3.1. Simulated vegetation

The potential vegetation cover of Europe at 6 ka, simulated by LPJ-GUESS, is dominated by forests according to all modelled scenarios (Fig. 2). Evergreen trees (ET) prevail in central and eastern Europe, while summergreen trees (ST) dominate western Europe. The simulated land cover of southern Europe is largely open, depending on the model scenario. The simulation using the coarser-scale EC-Earth climate data as the input does not show dominance of bare ground anywhere. The high-resolution RCM-based simulations L1 and L2 suggest that large parts of the Scandinavian mountains were covered by very sparse vegetation. This difference between the global and regional models is related to differences in elevation where the high-resolution RCMs have higher elevations in the mountainous regions, and therefore also represent colder and less favourable conditions. This is also indicated by larger fractions of non-vegetated areas in other mountainous regions including the Alps. There are also important differences between L1 and L2 in Scandinavia. This is a consequence of the different climate scenarios simulated by RCA4 (L1) and HCLIM (L2). L1 shows larger areas of bare ground in the mountain range, and a generally more open landscape in northern Sweden and Finland; while L2 shows more extensive bare ground in the Kola peninsula (in the far north east of the domain), as well as forests dominated by ET extending further north.

The reconstructed land cover (R) shows less latitude-dependant zonal vegetation composition than model-simulated vegetation across all of Europe. Mixed forests with both ST and ET are dominant, with ET more abundant in northern and eastern Europe, while ST is more abundant in western Europe. Moreover, R indicates more open land (larger cover of OL) than simulated by LPJ-GUESS, except in the southernmost regions. Although the EC-Earth/LPJ-GUESS-simulated bare ground has been accounted for in R, by increasing OL at the expense of ET and ST, the overestimation of ET (mainly pine), in the Alps, the Scandinavian mountains and northernmost Scandinavia is a pollen-based bias not entirely corrected by REVEALS (Binney et al., 2011; Trondman et al., 2015), which is not completely removed.

3.2. Simulated climate

Fig. 3 shows the simulated differences between 6 ka and PI climate. Here we discuss only the 6k-R runs (based on REVEALS reconstructed vegetation) since they use the most realistic land-cover data. The impact of different vegetation is discussed in section 3.3. In winter, all simulations concur that 6 ka was warmer than the PI period, and all simulations provide a similar pattern, with the smallest differences in temperature at 2 m over the Iberian Peninsula (0.5–1.5 °C) and the largest in north-eastern Europe (4–7 °C). EC-Earth is in the lower end of this range, showing differences of around 1 °C less than RCA4 and around 2 °C less than HCLIM for most of Europe. In parts of Scandinavia and Russia the differences in HCLIM are smaller than in RCA4, and for some locations even smaller than in EC-Earth. In summer the smallest differences are also found over the Iberian Peninsula and western Europe, and the largest differences are found in south-eastern Europe as well as in areas close to the sea-ice margin in the far north. The difference between RCA4 and HCLIM is larger in summer, although the temperature pattern is similar in both models. While the temperature differences between 6k-R and PI span 0.5–3.5 °C in HCLIM, the differences in RCA4 are close to zero in western Europe, and not more than 2 °C in the southeast. EC-Earth lies between the RCMs with very small variations between parts of Europe.

Generally, 6k-R is wetter than PI in winter, especially in western and northern Europe where 6 ka is 10–25% wetter in all three models (Fig. 4). Some regions in central Europe and the Mediterranean have small or even negative differences of up to 10%. In summer, there is a clear distinction between northern and southern Europe. In most of northern Europe 6 ka is wetter by more than 25%, whereas in large parts of southern Europe 6 ka is at least 25% drier. The precipitation patterns are similar in all three models, although with higher amplitudes in the RCMs, which suggests that precipitation is mostly governed by the driving GCM and less by the RCMs. This strong dependency of precipitation changes on the large-scale circulation as given by the GCMs is a well-known feature seen also in projections of future climate change (e.g. Kjellström et al., 2018; Christensen and Kjellström, 2020).

Fig. 5 shows sea level pressure (SLP) at PI and the difference between 6 ka and PI. In winter the SLP over Scandinavia is clearly lower in the RCMs compared to in EC-Earth. This indicates that low-pressure systems have a stronger influence in eastern parts of the Atlantic sector in the RCMs than in EC-Earth. Comparing the two time periods it is clear that SLP is lower at 6 ka over Scandinavia and northeastern Europe, which implies enhanced cyclone activity. This tendency of lower 6 ka SLP differs between EC-Earth and the RCMs: it is stronger in EC-Earth over the easternmost parts of the domain while both RCMs show stronger negative anomalies over large parts of the north Atlantic. Such differences between the RCMs and the driving global climate model may partly explain differences in precipitation anomalies between the models. For instance, the stronger SLP anomaly over the easternmost part of the domain in EC-Earth compared to the RCMs may be related to the larger positive precipitation anomaly in that region (cf. Fig. 5). The RCMs, on the other hand, show that stronger precipitation anomalies are further north, including the Baltic Sea area. Over parts of the North Atlantic, the RCMs indicate more precipitation associated with lower SLP.

In summer, the Icelandic low is located further to the south at 6 ka, which means stronger westerlies on average and increased low pressure activity over the North Atlantic and western Europe. This is reflected in the higher precipitation seen at 6 ka in western

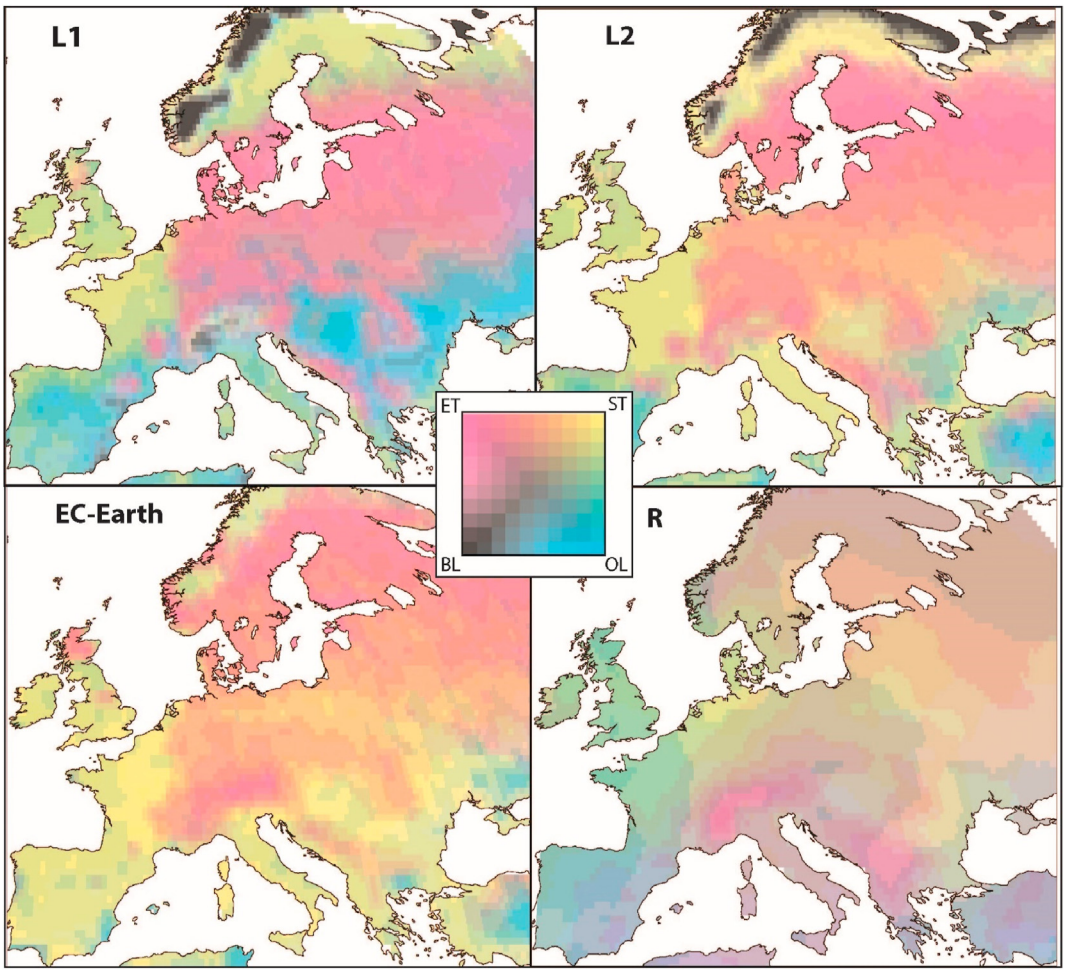

Fig. 2. Composite maps of LPJ-GUESS simulated potential natural vegetation cover using climate inputs derived from different climate models (L1 – RCA4, L2 - HCLIM, EC-Earth) and reconstructed vegetation cover (R) of Europe at 6 ka.
Legend: ET – evergreen forest; ST– summergreen forest; OL – open landcover; BL – bare ground.

Europe (cf. Fig. 4). The larger precipitation anomalies seen in the RCMs correspond to larger pressure anomalies. SLP is also slightly lower in the Mediterranean region. In this region, higher temperatures lead to a decrease in soil moisture, and therefore do not lead to increased precipitation. In the far north, on the other hand, the somewhat higher sea level pressure at 6 ka is indicative of a weaker pressure gradient and, consequently, less cyclonic activity which can partly be seen as reduced rainfall in some areas – close to the Norwegian coast and west of Iceland.

3.3. Climate response to changes in vegetation – the importance of ALCC

In this section the 6k-R runs described in section 3.2 will be used as the reference and compared to the 6k-L1 and 6k-L2 runs, i.e. we discuss the climate difference (6k-L1) – (6k-R) and (6k-L2) – (6k-R), abbreviated L1-R and L2-R below (Table 1). In this way we will see how RCA4 and HCLIM respond to the changes in vegetation indicated by Fig. 2. Here we show the surface temperature instead of the diagnostic 2 m-temperature, which is defined in different ways depending on the model, and may represent different things (Breil et al., 2020). Surface temperature has a common definition, and correlates better to differences in radiation and heat fluxes. Differences are tested using a student's t-test with Bonferoni (1936) correction for multiple testing. The resulting procedure has a 5% family-wise error rate, i.e. the probability of one or more false positives among all grid cells is 5%; instead of the 5% false positive rate for each individual grid cell obtained when no correction is applied.

L1-R differences in winter surface temperatures are very small in both RCA4 and HCLIM simulations in western and southern Europe, which is expected given the small differences in L1 and R vegetation in these regions. L1-R temperature differences are within ±0.5 °C, if at all significant. In areas with more pronounced L1-R differences in land cover, such as central and north-eastern Europe and the Alps, the L1-R differences in winter temperature are larger, up to 1 °C in RCA4 and 2 °C in HCLIM (Fig. 6). In Scandinavia and to some extent the Iberian Peninsula, 6k-L1 and 6k-L2 are colder than 6k-R. The response in 6k-L2 in HCLIM is particularly strong, up to 3 °C colder.

For both L1 and L2 the albedo difference is similar, but not the same, in RCA4 and HCLIM. The most notable differences are found around the Mediterranean, where the L1-R and L2-R albedo difference is negative in RCA4 and positive in HCLIM (Fig. 7). The differences in winter and spring surface temperatures are correlated with the differences in albedo (Fig. 7). Surface temperatures are generally reduced where albedo is increased and increased where albedo is reduced. RCA4 is not very sensitive to differences in albedo between L1, L2 and R in winter, and shows significant L1-R and L2-R differences in temperature only in the Alps and the

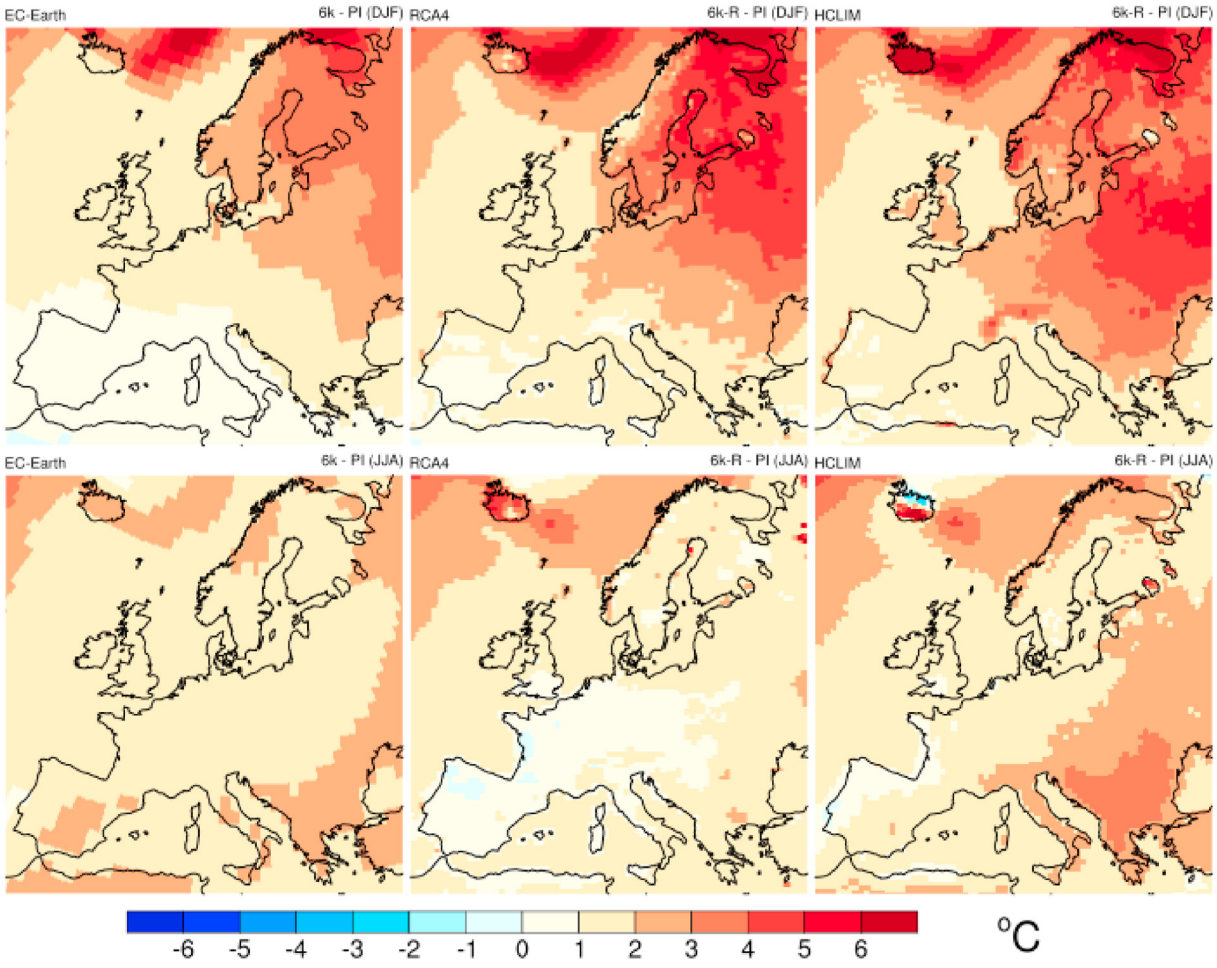

Fig. 3. Temperature difference (°C) between 6k-R and PI for winter (DJF, top row) and summer (JJA, bottom row) for EC-Earth (left), RCA4 (middle) and HCLIM (right).

Carpathians. Since these are mountainous regions, it seems likely that the temperature differences are connected to snow cover rather than directly to the albedo of different vegetation types. Landscapes that are more open are more readily covered with snow, which means that albedo is extra high during the snow season. This will further increase the difference in winter and spring albedo between forests and open land; which in turn increases the difference in temperature (e.g. Gao et al., 2014; Strandberg and Kjellström, 2019; Davin et al., 2020). HCLIM shows a stronger response in winter temperature. Both L1-R and L2-R differences are 0.5–1 °C in large parts of central and eastern Europe. The largest differences in albedo are seen in the Scandinavian mountains. In the L2 vegetation a large part of the Scandinavian mountain range is non-vegetated (Fig. 2). Therefore, the L2-R albedo differences, and thus the L2-R temperature differences, are larger than the L1-R differences. The L1 vegetation used in the 6k-L1 simulations has larger vegetation-covered areas in the Scandinavian mountain range. At high latitudes the albedo effect is strongest in spring, since the snow season is longer and the winter insolation is weak. In HCLIM 6k-L1 is 0.5–1.5 °C warmer than 6k-R in central Scandinavia in spring (March–May, see Fig. S1 in Appendix A), corresponding to a negative L1-R albedo difference in the region. 6k-L2 is 1–3 °C colder than 6k-R in the Scandinavian mountain range, corresponding to a positive L2-R albedo difference in this region (Fig. S1 in Appendix A).

In summer, RCA4 and HCLIM respond differently to changes in vegetation (Fig. 8). The differences are small, but significant for large parts of Europe. For RCA4, both 6k-L1 and 6k-L2 are around 0.5 °C colder than 6k-R. The only large difference between 6k-L1 and 6k-L2 for RCA4 is over the Scandinavian mountains. This region is less forested in 6k-L2 than in 6k-L1, which leads to even larger temperature differences compared to 6k-R, which shows the smallest fraction of open land in this area. In HCLIM, both 6k-L1 and 6k-L2 are warmer than 6k-R in summer in central and eastern Europe, and colder in the south and north. The differences are rather small, mostly within ±0.5 °C.

Differences in summer surface temperature are opposite to differences in evapotranspiration in both RCA4 and HCLIM (Fig. 9). A larger forest fraction gives increased evapotranspiration, which lowers surface temperature. Conversely, a smaller forest fraction gives decreased evapotranspiration, which elevates the surface temperature. In southern Europe 6k-L1 and 6k-L2 are colder than 6k-R due to positive L1-R and L2-R differences in evapotranspiration from the denser forest in 6k-L1 and 6k-L2 compared to 6k-R; 5–15% more evapotranspiration in HCLIM and up to 20% more in RCA4. In northern Scandinavia, 6k-L1 and 6k-L2 are colder despite the smaller forest fraction and lower evapotranspiration. The mountain regions do sometimes have snow during summer, which means that albedo is also an important factor in summer (JJA). In addition, the cold climate generally leads to reduced evapotranspiration and thus reduces the potential for changes in land cover to affect temperature.

Significant L1-R and L2-R summer evapotranspiration differences are seen in northern Scandinavia and around the

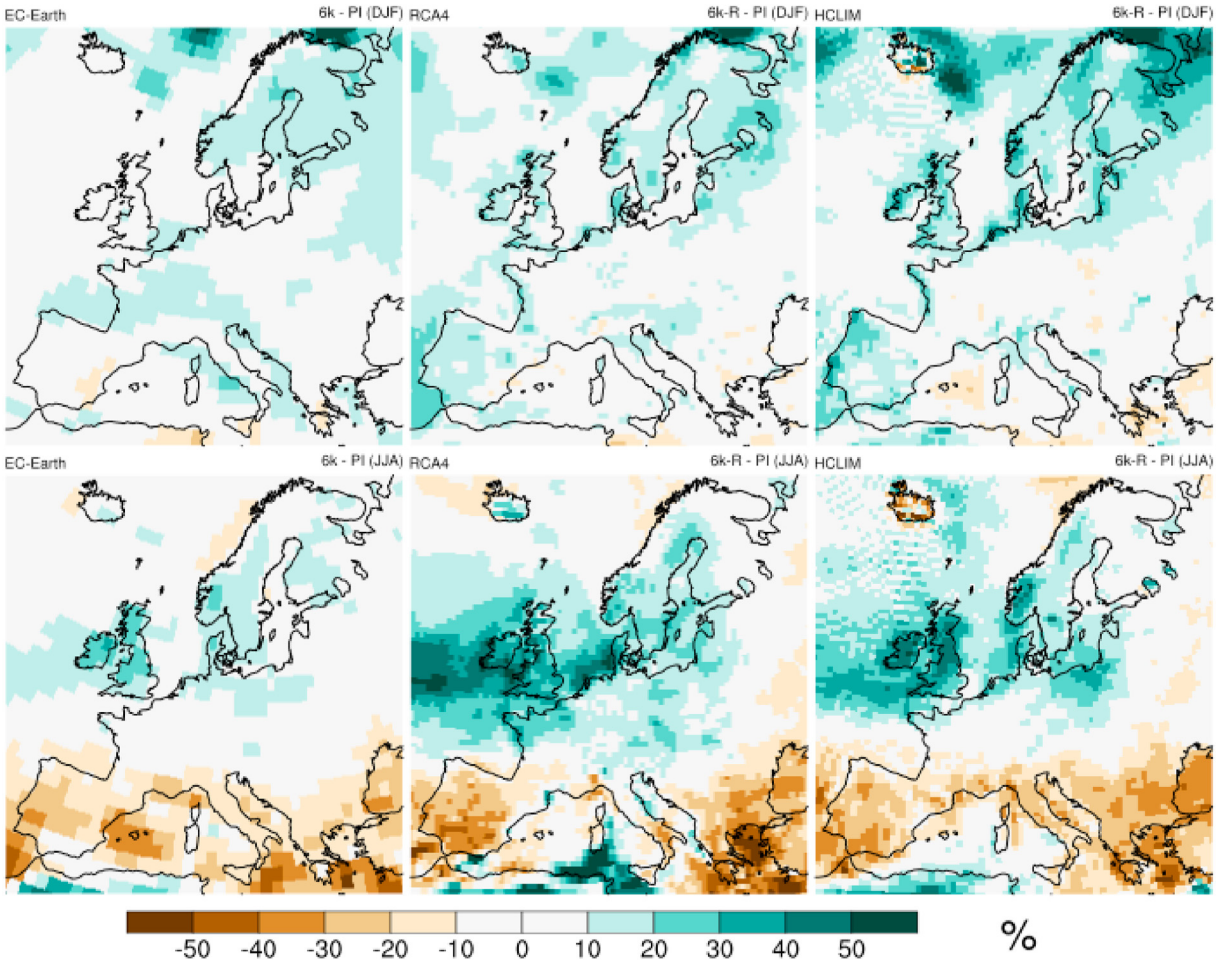

Fig. 4. Precipitation difference (%) between 6k-R and PI for winter (DJF, top row) and summer (JJA, bottom row) for EC-Earth (left), RCA4 (middle) and HCLIM (right).

Mediterranean. In Scandinavia, less evapotranspiration in L1 and L2 is connected to the larger degree of open land. In the South, only RCA4 shows large-scale significant differences. Positive L1-R and L2-R evaporation differences are connected to more extensive forest fractions in this region. Strandberg et al. (2014) noted that the albedo effect also dominates in southern Europe in summer in their study based on RCA3. The already dry soils prevent changes in evapotranspiration regardless of changes in land cover. We see a tendency towards such an effect in small areas in the southwestern part of the Iberian Peninsula in RCA4 and parts of Italy and southwestern Iberia in HCLIM. This effect is suggested to be stronger when the forest fraction is reduced to below 20% (Strandberg et al., 2014), which is not the case in these simulations.

The studied vegetation changes have only little effect on precipitation (Figs. S2 & S3 in Appendix A). With larger forest fraction, the surface roughness is higher. The increased friction leads to stronger convergence, which in turn leads to more precipitation (Belušić et al., 2019). There is such a tendency, but differences in precipitation are essentially insignificant everywhere.

4. Discussion

4.1. Differences in land-cover descriptions – cause and effects

Simulated (L1 and L2) and reconstructed (R) land cover exhibit clear compositional differences. It must be kept in mind that the DVM simulated potential natural vegetation in this study is entirely determined by prescribed simulated climate, i.e. the simulations do not account for the effects of LULCC. The reconstructed land cover, in contrast, is a pollen-based reconstruction of the actual vegetation, that is a product of complex interactions between several natural and anthropogenic factors including the actual climate. However, LULCC do not explain all differences between R and L1 or L2. L1 and L2 are two sets of DVM simulated natural potential vegetation differing only in input climate that is taken from two different RCMs. The pollen-based reconstructed land cover R is a result from the actual climate at 6 ka and human impact on vegetation. Thus, differences between R and L1 or L2 can also be due to differences between the actual climate and the RCM-simulated climates. This implies that some differences can be due to LULCC while others can be due to differences between simulated and actual climates and to weaknesses in the applied methods. The R land cover suggests that the largest LULCC at 6 ka occurred in southern and western Europe, in agreement with an earlier REVEALS reconstruction of land cover in Europe (Trondman et al., 2015) and with LULCC scenarios (Kaplan et al., 2010, 2017). Thus, it is unlikely that the differences between R and L1 or L2 in Scandinavia mainly are caused by LULCC. Therefore, the difference in climate in this region between 6k-R and 6k-L1 or 6k-L2 is most probably not an effect of anthropogenic changes in this part of Europe, but rather an effect of how 6 ka climate is represented in LPJ-GUESS and REVEALS. In southern Europe, however, differences in climate might be a response to LULCC. The 6 ka – PI difference in summer temperature is amplified by 0.5° when R vegetation is

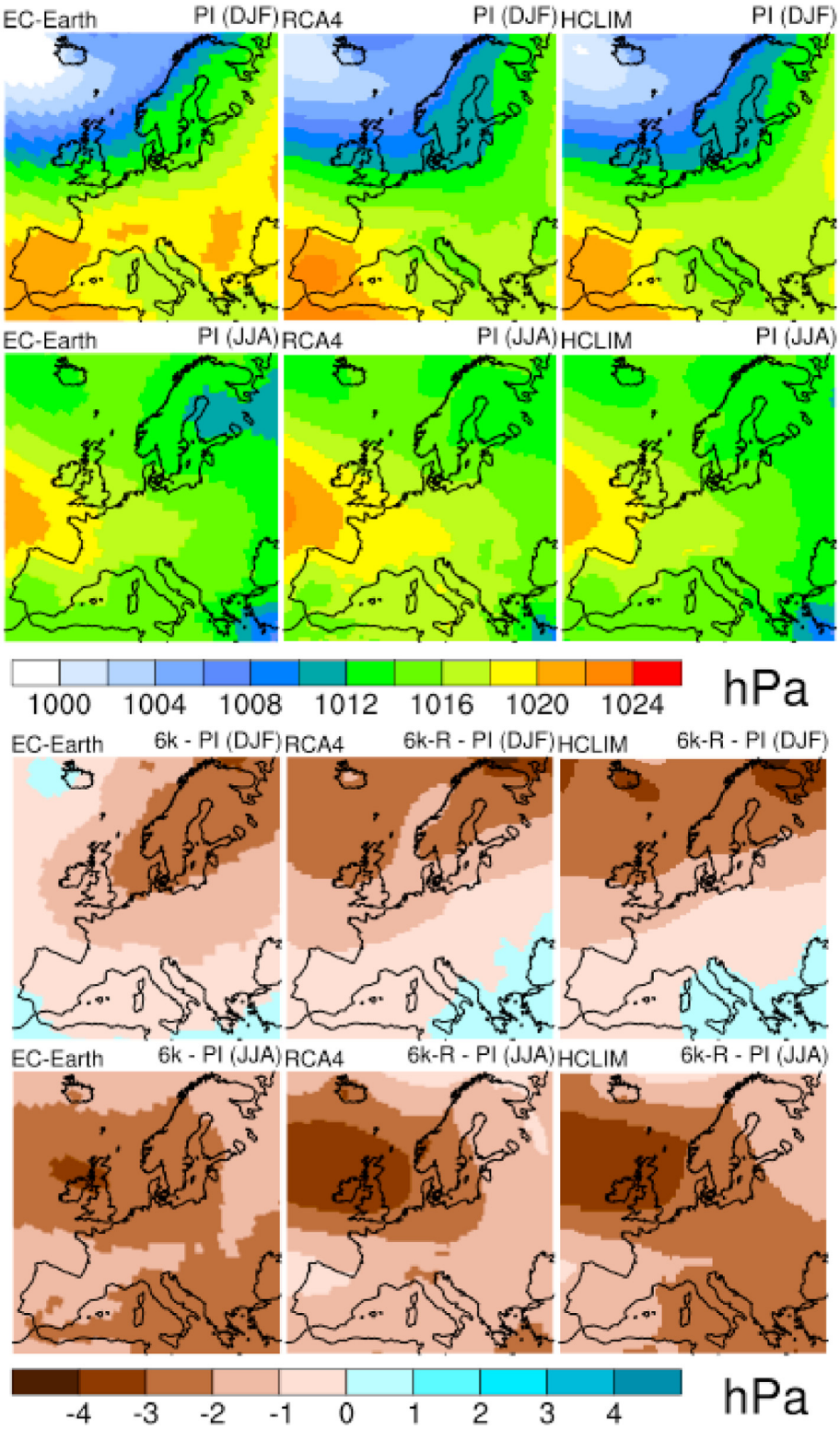

Fig. 5. PI sea level pressure (hPa) in winter (DJF, first row) and summer (JJA, second row). Difference in sea level pressure (hPa) between 6k-R and PI in winter (DJF, third row) and summer (JJA, fourth row). EC-Earth (left), RCA4 (middle) and HCLIM (right).

used. The extent of this effect is highly model dependent. The RCA4-simulated 6k-R climate is warmer in most of southern Europe, while the HCLIM-simulated 6k-R climate exhibit significant temperature differences only in parts of the Iberian and Balkan Peninsulas.

4.2. RCM simulated climates compared to proxies

In the comparison between model results and reconstructed climate, we first exclude purely pollen based proxies, as our results are based on pollen data to some extent. This allows us to avoid

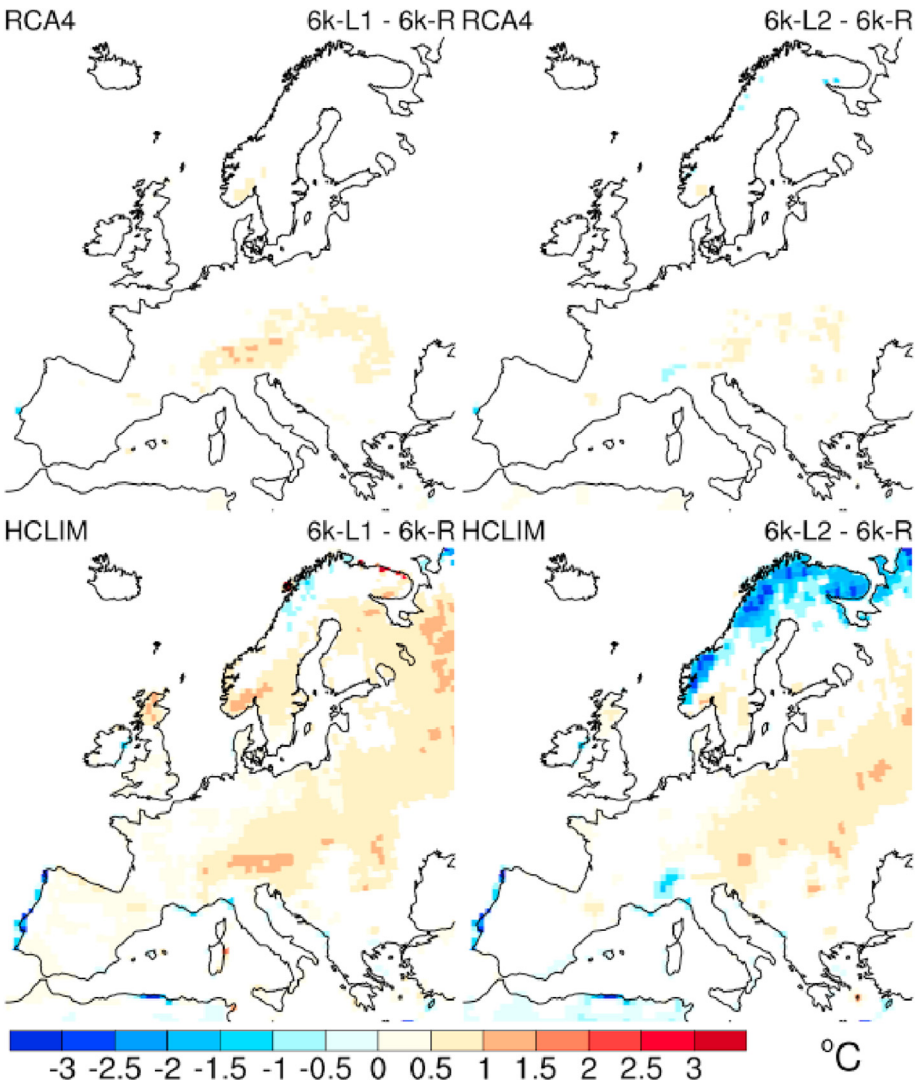

Fig. 6. Difference in surface temperature (°C) in winter for RCA4 (top row) and HCLIM (bottom row) between 6k-L1 and 6k-R (left column) and 6k-L2 and 6k-R (right column). Only grid cells that show a significant difference on a 0.05 level are coloured.

circular reasoning in model-data comparison. Studies of diatoms (Korhola et al., 2000; Rosén et al., 2001; Bigler et al., 2006; Heinrichs et al., 2006; Shala et al., 2017), tree rings (Grudd, 2002; Helama et al., 2002) and chironomids (Rosén et al., 2001; Bigler et al., 2003; Hammarlund et al., 2004; Laroque and Hall, 2004; Velle et al., 2005; Heinrichs et al., 2008; Luoto et al., 2010; Shala et al., 2017) indicate a 6 ka − PI difference in summer temperature of 0.5–2 °C in Scandinavia, which corresponds with our simulations (cf. Fig. 3). Evidence from the presence of Mediterranean ostracods in the coastal waters of Denmark suggests that winter temperatures at 6 ka were up to 4–5 °C above present (Vork and Thomsen, 1996). Our model results do not show such a large temperature increase, but it is nevertheless clear that the difference 6 ka − PI is larger in winter than in summer. Non-pollen proxies are scarce in central Europe. Diaconou et al. (2017) report around 0.5 °C colder summers in Romania based on chironomids, while Larocque-Tobler et al. (2009) and Heiri and Lotter (2005) found 0.5–1 °C warmer summers in Switzerland. Persoiu et al. (2017) do not present quantitative estimates, but based on stable isotope analysis they report warmer winters in central Europe and colder winters in eastern Europe. This is somewhat in conflict with our model results as 6 ka is simulated to be warmer than PI during all seasons for practically all of Europe.

Proxy records of relative precipitation indicate a drier climate at 6 ka than at PI in Scandinavia (Digerfeldt, 1998; Ikonen, 1993; Snowball and Sandgren, 1996; Hammarlund et al., 2003; Borgmark, 2005; Olsen et al., 2010), northern Germany (Niggeman et al., 2003), the UK (Hughes et al., 2000) and the western Mediterranean (Walczak et al., 2015; Persoiu et al., 2017), while there is no detectable difference in the Alps (Magny, 2004) and wetter conditions in eastern Europe (Persoiu et al., 2017; Galka and Apolinarska, 2014). This contrasts with the present model results that show wetter conditions in the north and west and drier in the south. This is not explained by the fact that many estimates based on biological proxies reflect effective precipitation (the relationship between precipitation and evapotranspiration). The models yield small differences or increases in effective precipitation, depending on model and season. The fact that the models indicate warmer and wetter conditions than the proxies is a general feature of the CMIP5/PMIP3 global simulations of the mid-Holocene PI climates (Harrison et al., 2015; Barthlein et al., 2017). The accepted explanation for this is the too weak zonal flows, and thus too weak moisture transport in the GCMs; which is reasonable given the approximate 2° × 2° resolution in PMIP3.

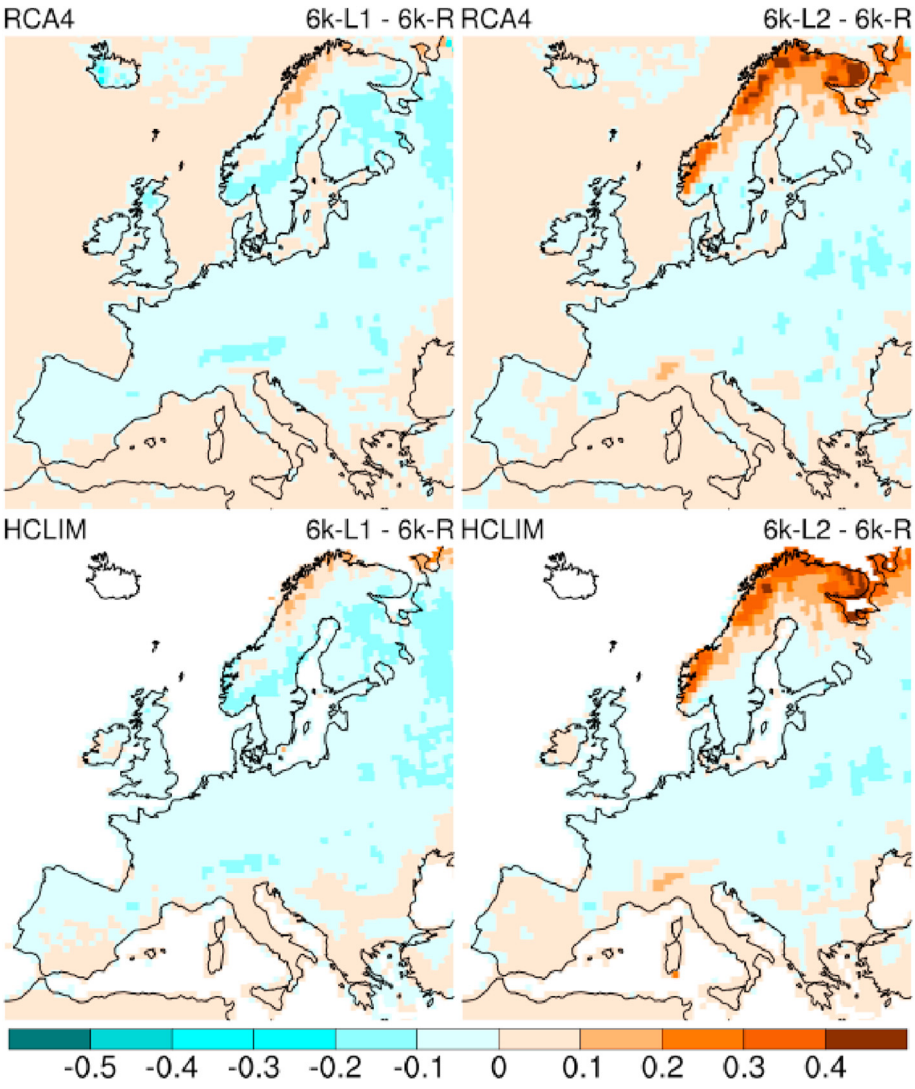

Fig. 7. Difference in albedo in winter for RCA4 (top row) and HCLIM (bottom row) between 6k-L1 and 6k-R (left column) and 6k-L2 and 6k-R (right column). Only grid cells that show a significant difference on a 0.05 level are coloured.

The only spatially extensive reconstructions are based on pollen data. Therefore, after having compared with other independent proxy data above, we make a deviation from the principle of not comparing with pollen-based data. This is done bearing in mind that the R vegetation in our simulations is based on pollen data transformed into vegetation cover. Mauri et al. (2014) (henceforth M14) presented a gridded reconstruction of 6k-PI for all of Europe. M14 reveals the largest temperature difference in Scandinavia (especially in winter), and a gradient with smaller differences between 6 ka and PI towards the south west. In M14, 6 ka is colder than PI over the Iberian Peninsula and most of the Mediterranean. Our simulations show a similar pattern in northern Europe. In southern Europe the differences are small and mostly positive; other than for a few regions in RCA4 in summer (Fig. 3). Precipitation conditions in winter are generally wetter in the northeast, in line with our simulations, but drier in the west, which is in disagreement with our results. In summer M14 identified a near opposite pattern as those in our simulations with drier conditions in Scandinavia and wetter in the southeast of Europe.

The result showing that 6 ka was warmer and wetter (at least in winter) than PI in Fennoscandia is a robust outcome supported by most proxies and climate models. For the rest of Europe, the results presented here do not agree as clearly with other proxies and reconstructions. However, proxy reconstructions are sparse for central and southern Europe and also less consistent with each other. Both Perciou et al. (2017) and Peyron et al. (2017) state that the Mediterranean 6 ka climate was mostly wetter than PI, but with large geographical variation. This is in some conflict with the precipitation differences presented in this study, which are mostly drier.

4.3. Differences between 6 ka and PI climates - comparison with previous studies

The simulations presented here are compared with results from 9 PMIP3 models (Braconnot et al., 2012) as well as data from M14 and Strandberg et al. (2014, henceforth S14). The PMIP3 models used are: BCC-CSM1-1 (Wu et al., 2014); CNRM-CM5 (Voldoire et al., 2012); CSIRO-Mk3-6-0 (Rotstayn et al., 2012); FGOALS-GS (Li et al., 2013); GISS-E2-R (Schmidt et al., 2014); IPSL-CM5A-LR (Dufresne et al., 2013); MIROC-ESM (Watanabe et al., 2011); MPI-ESM-P (Stevens et al., 2013); and MRI-CGCM3 (Yukimoto et al., 2012). S14 simulated 6 ka climate with an approach similar to the present, for example, by using RCA3 in combination with LPJ-GUESS.

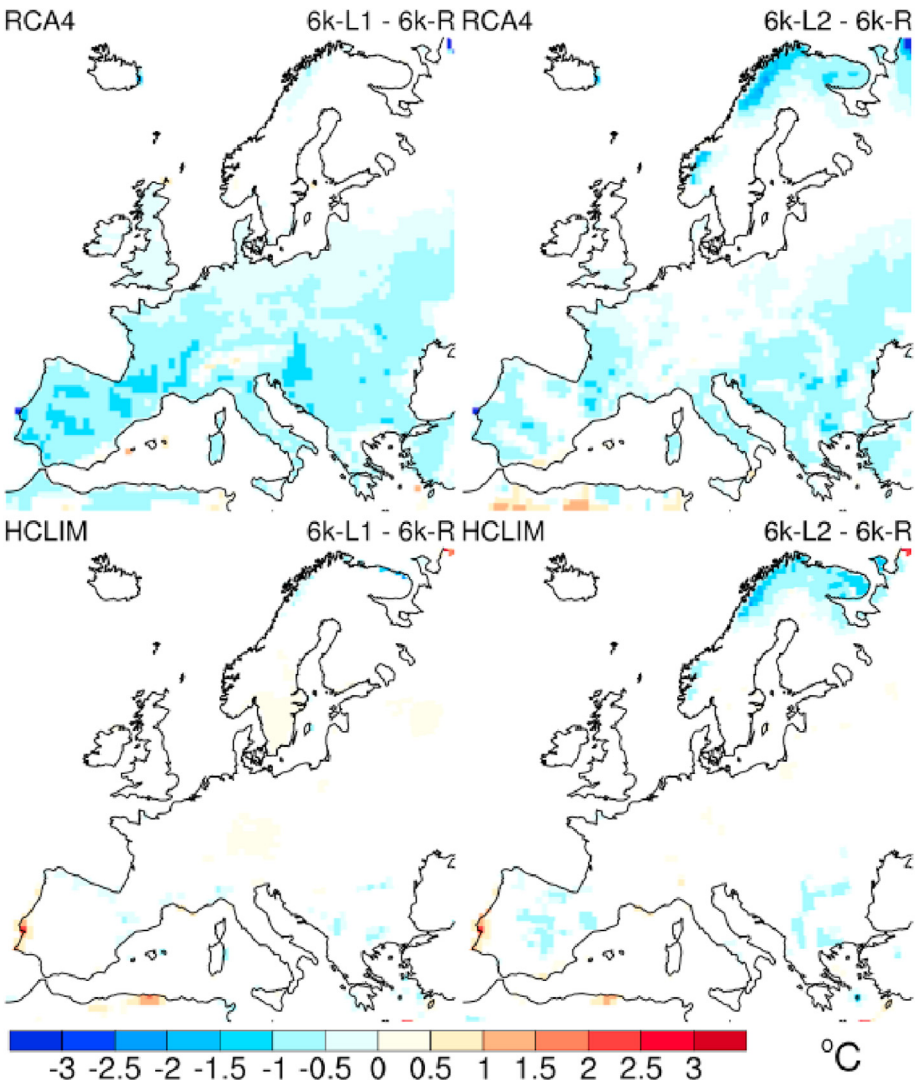

Fig. 8. Difference in surface temperature (°C) in summer for RCA4 (top row) and HCLIM (bottom row) between 6k-L1 and 6k-R (left column) and 6k-L2 and 6k-R (right column). Only grid cells that show a significant difference on a 0.05 level are coloured.

Fig. 10 shows the differences in temperature and precipitation between 6 ka and PI for northern Europe (NEUR, -10 - 34 E, 50–70 N) and southern Europe (SEUR, -8 - 24 E, 35–50 N) from the GCM and RCMs (6k-R) used in this study, the PMIP3 and PMIP4 GCMs, the S14 RCM and the reconstruction from M14. There is some spread between the PMIP3 models and a larger spread between PMIP4 models, especially for temperature. The difference in precipitation between 6 ka and PI is at the most between −0.2 mm/day and +0.2 mm/day, with the exception of one PMIP4 model that reaches up to 0.4 mm/day. The difference in temperature is at the most between −1 °C and 2 °C. The models used here, EC-Earth3-LR, RCA4 and HCLIM give a considerably larger 6 ka-PI difference than the PMIP3 models, but is within the range of PMIP4 for exept for winter in northern Europe. The temperature difference is never less than 1 °C, and in northern European winter this is almost 4 °C. In northern Europe, the precipitation differences are also considerably larger. RCA4 and HCLIM are in close agreement with the driving EC-Earth, but are not identical. Using different models would give different results, but not change the overall conclusions, although within the PMIP4 ensemble EC-Earth-LR is the model that shows the largest winter warming in northern Europe. In any case, it is difficult to say which model would be the best representing 6 ka climate conditions. Brierley et al. (2020) report a PMIP4 6 ka − PI precipitation difference similar to PMIP3 in Europe. For temperature, Brierley et al. (2020) show that PMIP3 and PMIP4 are similar; the largest exception is that the difference in summer temperature between 6 ka and PI in northern Europe is smaller in PMIP4 than in PMIP3.

S14 simulated a 6 ka climate that was warmer than PI by 2–3 °C at the most (the largest differences were identified in northern Europe in winter and southern Europe in summer). For winter, we obtain a similar temperature difference between 6 ka and PI as S14 with a gradient from the northeast, which is around 3 °C warmer than the southwest where the 6 ka-PI difference is close to zero. In summer, we identify a small positive 6 ka-PI difference in the southwest, where S14 show a 6 ka climate that is up to 3 °C warmer than PI. Since RCA3 and the driving ECHO-G in S14 simulate similar climates (Fig. 12 in S14), the differences between S14 and the present study are mostly explained by the different driving GCMs (EC-Earth in this study). For precipitation, the current results agree with S14 in terms of wetter winter conditions at 6 ka than PI in the north and south and 6 ka-PI differences in precipitation close to zero in central Europe. Contrastingly, the results are almost opposite for summer precipitation. While in this study 6 ka is characterized by

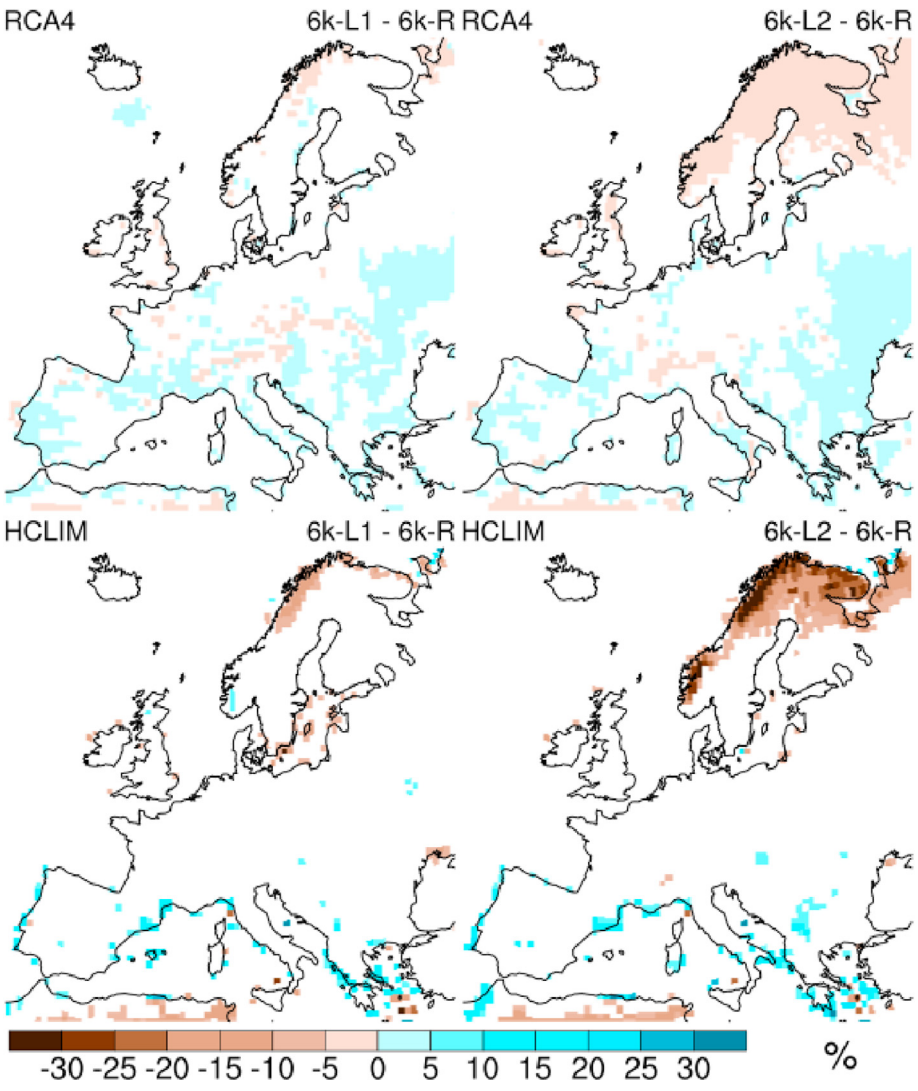

Fig. 9. Difference in evapotranspiration (%) in summer for RCA4 (top row) and HCLIM (bottom row) between 6k-L1 and 6k-R (left column) and 6k-L2 and 6k-R (right column). Only grid cells that show a significant difference on a 0.05 level are coloured.

wetter conditions than PI in the north and drier in the south, S14 identified drier conditions in the north and somewhat wetter in the southeast. Russo & Cubash. (2016, R16) simulated the 6 ka-PI difference by using the regional climate model COSMO-CLM forced by ECHO-G (same GCM run as in S14). For winter they simulated warmer 6 ka conditions in Scandinavia and the British Isles, and colder conditions in the southeast of Europe. The results of the present study match the clearly warmer conditions in Scandinavia and the small 6 ka-PI differences over the Iberian Peninsula. For summer, R16 simulated warmer conditions across Europe at 6 ka comparable to both S14 and the present study, but without any large variations between different parts of Europe.

Fig. 10 summarizes the differences between 6 ka and PI climates from the studies described above. All models agree that 6 ka was warmer than PI with the possible exception of southern European winter where the PMIP3 ensemble and S14 is close to 0 °C. 6 ka is mostly wetter in winter, while the summer precipitation differences are evenly spread around 0 mm/day. The only dataset providing proxy-based area averages is M14. For precipitation, M14 is within the spread of the models. For temperature, M14 is clearly different. In M14, 6k is colder than PI in large parts of southern Europe. This obvious mismatch between model simulations and reconstructions points to the issue of the 'Holocene temperature conundrum' (HTC, Liu et al., 2014; Bader et al., 2020). There are regions with major discrepancies between simulated and reconstructed climates across the globe (Mauri et al., 2014; Harrison et al., 2015; Bartlein et al., 2017). Our result support the idea that 6 ka was clearly warmer than PI in Europe. The differences between the experiments in this study, however, are minor compared to the differences to other studies. The inclusion of LULCC in the simulations does not affect this comparison. This shows how the simulated climate is highly dependent on the models used, especially when forcing conditions are less constrained compared to present climate.

4.4. Robustness of the results

Simulated climate scenarios depend on the climate model(s) used, but the response to differences in vegetation can also differ significantly between models. Natural internal variability may, therefore, be a reason for why our results differ from other model studies or from reconstructions based on proxy data. For current climate conditions, Davin et al. (2020) and Breil et al. (2020) studied the response to idealized vegetation changes in several RCMs (of

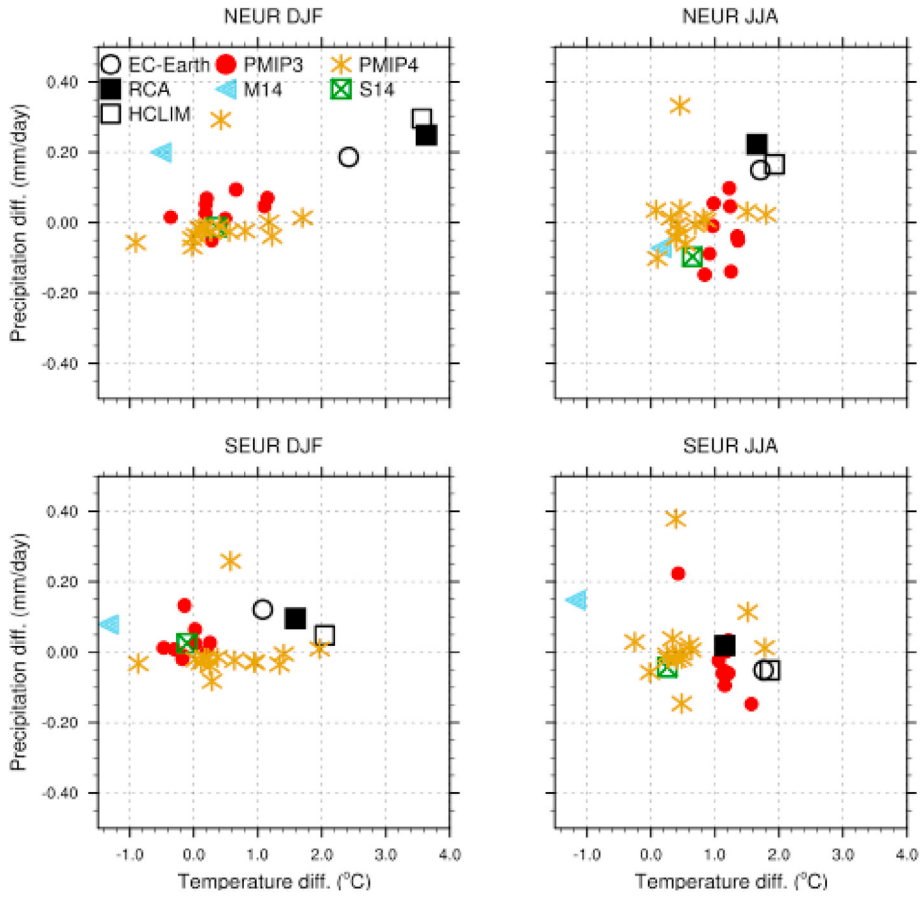

Fig. 10. Difference in temperature (°C) and precipitation (mm/day) between 6 ka and PI (6 ka − PI) in northern Europe (NEUR, top row) and southern Europe (SEUR, bottom row) for winter (DJF, left column) and summer (JJA, right column). The simulations in this study using 6k-R vegetation are represented by open circles (EC-Earth3-LR), filled squares (RCA4) and open squares (HCLIM). Red dots represent PMIP3 models, gold stars PMIP4 models, blue triangles data show from Mauri et al. (2014, M14) and green crossed squares show data from Strandberg et al. (2014, S14).

which RCA4 was one). All models agree on the response in albedo and temperature in winter, but in summer the response in heat flux and temperature, for example, can have different signs. As an example, Russo et al. (2021) show that a RCM can be sensitive to perturbations of the soil moisture, and that land-surface interactions can explain some of the discrepancies between models and proxies for mid-Holocene summer temperature in Europe. We would have reached different results if we had used other models. We try to limit the impacts by using two models with different model physics. We can, to some extent, describe uncertainty associated with responses to vegetation changes due to model physics, as we get the same kind of different responses as Davin et al. (2020) and Breil et al. (2020). However, we acknowledge that we do not represent the full uncertainty and envisage future more comprehensive studies including a larger variety of climate models to better assess these differences.

Summer insolation at 50°N was around 25 W/m^2 higher at 6 ka than at PI while winter insolation was 5–10 W/m^2 lower (Fischer and Jungclaus, 2011; Xu et al., 2020). Insolation changes explain differences between 6 ka and PI climate in summer (e.g. Russo and Cubash, 2016), although alterations in atmospheric circulation may also impact climate (e.g. Mauri et al., 2014). These differences in insolation are included in EC-Earth, but not explicitly in the RCMs. As lateral boundary conditions and sea surface conditions used in the RCMs are taken from EC-Earth, the resulting climate in the RCMs indirectly takes into account part of the differences in insolation between the two periods. Similar inconsistencies between RCMs and their driving GCMs has been discussed for other forcing agents and other time periods. Differences between present-day and future climate conditions in RCMs with constant concentrations of greenhouse gases or aerosols has been shown to differ from that of their driving GCMs where these are changed with time (e.g. Jerez et al., 2018; Boé et al., 2020). From our results we note that the RCMs have smaller temperature differences than EC-Earth in western Europe in summer (Fig. 3), which could potentially be a result of the smaller insolation differences. For eastern Europe the results are ambiguous, with RCA4 showing smaller temperature differences compared to EC-Earth while HCLIM shows larger differences. These differences indicate that the results are sensitive not only to changes in forcing factors, but also model-specific formulations of physical processes, resulting in different feedback. For most ocean areas differences between EC-Earth and the RCMs are small, as the RCMs are strongly governed by the EC-Earth sea-surface temperatures. We conclude that the missing description of accurate insolation at 6 ka in the RCMs affects the simulated 6 ka climate. For parts of the domain, this has likely an impact on the results. Determining the extent of this impact, and how it may differ between different seasons and locations, is beyond the scope of this study and requires separate further work.

Different insolation could potentially also affect the simulated land cover since insolation has a direct effect on vegetation. Fig. 2 shows vegetation simulated using RCM climate and present insolation (L1 & L2), vegetation simulated using GCM climate and 6 ka insolation (EC-Earth) and reconstructed vegetation (R). The

differences between L1 and L2 tell us that simulated vegetation can be different even with the same insolation, because of differences in temperature and precipitation. Differences to the EC-Earth and R vegetation are the result of the forcing climate and insolation (and, in the case of reconstructed vegetation, the method used). It seems that the simulated vegetation is more affected by climate than insolation, but we have to acknowledge it as an uncertainty and suggest assessing sensitivity in vegetation models as a topic for future work.

5. Conclusions

This study describes mid-Holocene (at 6 ka) vegetation and climate as simulated by one GCM, two RCMs, one DVM and according to one reconstruction of 6 ka vegetation based on pollen data, statistical interpolation methods and climate model results, which indicates how climate is influenced by vegetation and LULCC, and how sensitive RCMs are to differences in land cover.

The models simulate a 6 ka climate that was warmer than PI climate. The largest differences are seen in Scandinavia in winter where the simulated 6 ka climate is 2–4 °C warmer than PI, a signal that is shared with proxy data and previous model studies. In summer, the difference between the simulated 6 ka and PI climates is smaller (0–3 °C) with the smallest differences in the southwest of Europe. The simulated 6 ka climate is wetter than PI by 10–30% in the north and the west. Around the Mediterranean, the simulated 6 ka climate is up to 20% drier in summer, but with a precipitation level similar to PI in winter. There is less agreement with other proxy records for precipitation, but the proxy datasets are also less consistent with one another. The PMIP3 ensemble also have members that give a positive 6 ka − PI precipitation difference as well as negative. There is at least some agreement between models and proxies regarding wetter 6 ka conditions in Scandinavia during winter, while for summer, models and proxies reveal opposite signals. The signal of a generally warmer 6 ka shown in this study matches other model studies (even though the magnitude of the difference is unusually large here), but not all proxy reconstructions. The mismatch between models and proxies connects to the issue of the HTC. This study cannot be used to make inferences about global temperature or temperature trends throughout the Holocene, but it clearly supports the notion of 6 ka being warmer (and wetter) than PI in Europe.

Simulated potential vegetation is dominated by forests: evergreen coniferous forests dominate in central and eastern Europe, while deciduous broadleaved forests dominate western Europe. Reconstructed land cover, however, shows mixed forests in northern and eastern Europe, and deciduous broadleaved forests in western Europe. Furthermore, compared to simulated potential natural vegetation, reconstructed vegetation cover is considerably more open in most of Europe.

The choice of vegetation has a significant impact on the simulated temperature. Winter and spring temperatures are closely related to albedo, which is largely the same in both RCMs, and which is strongly affected by vegetation in both. In summer, the RCMs used in this study respond somewhat differently to vegetation differences, showing that not only the choice of land cover, but also the choice of model, is important for the simulated climate. Summer temperatures are strongly related to differences in heat fluxes between the atmosphere and the ground. Since the response in heat fluxes to differences in land cover depends on model physics, it is more likely that models respond differently in summer than in winter. HCLIM responds more strongly to the imposed differences in vegetation than RCA4. This explains some of the differences between the climate conditions simulated by RCA4 and HCLIM, and also means that the choice of vegetation is even more important in HCLIM. It is unfortunately difficult to assess which model has the most realistic response. Proxy datasets are not consistent and have large uncertainties, and proxy-based climate reconstructions, especially quantitative records, are sparse for the 6 ka period. Furthermore, model performance is dependent on many other factors: such as large-scale circulation, parametrisations and resolution to name a few. The best way to manage this model uncertainty is to use several models to try to capture the range of possible climates. It should be noted that the choice of GCM is also an important contribution to the simulated climate. We were able to use only one GCM in this study, but we show that the use of another GCM would give different, but still comparable, results. The importance of the combination of GCM and RCM has been emphasised previously (e.g. Kjellström et al., 2018; Sørland et al., 2018), but has not been acknowledged sufficiently in downscaling exercises for past climates, even though there are recent studies using several GCMs or perturbed physics ensembles (Russo et al., 2021; Stadelmaier et al., 2021). The importance of model and vegetation choice calls for caution when designing palaeo climate experiments. Here we show that it is essential to have a good, well-motivated description of vegetation to simulate the same climate with different models in a model ensemble.

The climate change between 6 ka and PI is not only explained by variations in land cover. The distinctions are mainly explained by strong differences in solar insolation (e.g. Wanner et al., 2008; Renssen et al., 2009). This means that all models of quality will simulate similar 6 ka conditions, largely regardless of land cover. The differences in climate are small compared to other uncertainties in models and proxies. Nevertheless, the amount of LULCC used in this study (the difference between potential and reconstructed land cover) is large enough to exert a significant impact on the simulated climate. Consequently, it is likely that there was already an anthropogenic impact on European climate at 6 ka. We suggest that LULCC at 6 ka made parts of southern Europe around 0.5 °C warmer in summer. These relatively strong responses have some important implications:

i) Anthropogenic land cover changes may have already affected European temperatures at 6 ka.
ii) Simulated climate is sensitive to land cover. It is therefore important to use a land cover reconstruction that is both realistic and consistent with the simulated climate.
iii) Models respond to changes in land cover in different ways. It is therefore important to estimate model uncertainty by using model ensembles.
iv) Land cover-changes are also important for understanding future climate and should be included in simulations of the future.

Data availability

RCM data is available via the Bolin Centre Database https://doi.org/10.17043/strandberg-2022-landclim-ii-1.

DVM produced estimates of 6k land cover are stored in DataGURU (https://dataguru.lu.se/).

Credit author statement

Gustav Strandberg: Conceptualisation, Methodology, Formal analysis, Investigation, Writing – Original Draft, Visualisation; **Johan Lindström**: Conceptualisation, Methodology, Formal analysis, Investigation, Writing – Review & Editing; **Anneli Poska**: Conceptualisation, Methodology, Formal analysis, Investigation, Writing – Review & Editing, Visualisation; **Qiong Zhang**:

Conceptualisation, Methodology, Investigation, Writing – Review & Editing; **Ralph Fyfe**: Methodology, Formal analysis, Investigation, Writing – Review & Editing; **Esther Githumbi**: Conceptualisation, Methodology, Formal analysis, Investigation, Writing – Review & Editing; **Erik Kjellström**: Conceptualisation, Writing – Review & Editing ; **Florenze Mazier**: Methodology, Investigation, Writing – Review & Editing; **Anne Birgitte Nielsen**: Conceptualisation, Writing – Review & Editing; **Shinya Sugita**: Methodology, Writing – Review & Editing; **Anna-Kari Trondman**: Methodology, Investigation; **Jessie Woodbridge**: Methodology, Investigation, Writing – Review & Editing; **Marie-José Gaillard**: Conceptualisation, Writing – Review & Editing, Project administration, Funding acquisition.

Declaration of competing interest

The authors declare that they have no known competing financial interests or personal relationships that could have appeared to influence the work reported in this paper.

Acknowledgements

This study was funded by a research project financed by the Swedish Research Council VR (Vetenskapsrådet) on “Quantification of the bio-geophysical and biogeochemical forcings from anthropogenic de-forestation on regional Holocene climate in Europe, LandClim II”.

EC-Earth, RCA4 and HCLIM simulations and analyses were performed on the Swedish climate computing resource Bi provided by the Swedish National Infrastructure for Computing (SNIC) at the Swedish National Supercomputing Centre (NSC) at Linköping University. Financial support from the Linnaeus University's Faculty of Health and Life Science is acknowledged fikor Marie-José Gaillard, Anna-Kari Trondman, and Esther Githumbi. Qiong Zhang acknowledges financial support from the Swedish Research Council VR project 2013–06476 and 2017–04232. Anneli Poska acknowledges support by Estonian Research Council grant PRG323. This is a contribution to the strategic research areas MERGE (ModElling the Regional and Global Earth system), the Bolin Centre for Climate Research, and the PAGES LandCover6k working group that, in turn, received support from the Swiss National Science Foundation, US National Science Foundation, Swiss Academy of Sciences, and Chinese Academy of Sciences.

Appendix A. Supplementary data

Supplementary data to this article can be found online at https://doi.org/10.1016/j.quascirev.2022.107431.

References

Aitchison, J., 1986. The Statistical Analysis of Compositional Data. Chapman & Hall, Ltd, London.

Augustin, L., Barbante, C., Barnes, P., et al., 2010. Eight glacial cycles from an Antarctic ice core. Nature 429, 623–628. https://doi.org/10.1038/nature02599.

Bader, J., Jungclaus, J., Krivova, N., Lorenz, S., Maycock, A., Raddatz, T., Schmidt, H., Toohey, M., Wu, C.-J., Claussen, M., 2020. Global temperature modes shed light on the Holocene temperature conundrum. Nat. Commun. 4726, 11. https://doi.org/10.1038/s41467-020-18478-6.

Bartlein, P.J., Harrison, S.P., Brewer, S., Connor, S., Davis, B.A.S., Gajewski, K., Guiot, J., Harrison-Prentice, T.I., Henderson, A., Peyron, O., Prentice, I.C., Scholze, M., Seppä, H., Shuman, B., Sugita, S., Thompson, R.S., Viau, A.E., Williams, J., Wu, H., 2011. Pollen-based continental climate reconstructions at 6 and 21 ka: a global synthesis. Clim. Dynam. 37 (3–4), 775–802. https://doi.org/10.1007/s00382-010-0904-1.

Bartlein, P.J., Harrison, S.P., Izumi, K., 2017. Underlying causes of Eurasian mid-continental aridity in simulations of mid-Holocene climate. Geophys. Res. Lett. 44, 9020–9028. https://doi.org/10.1002/2017GL074476.

Bazile, E., Marquet, P., Bouteloup, Y., Bouyssel, F., 2012. The turbulent kinetic energy (TKE) scheme in the NWP models at meteo France. ECMWF, Shinfield Park, Reading, available at:. In: Workshop on Workshop on Diurnal Cycles and the Stable Boundary Layer, 7–10 November 2011, 127–135 (last access: 18 March 2020). https://www.ecmwf.int/node/8006.

Bechtold, P., Bazile, E., Guichard, F., Mascart, P., Richard, E., 2001. A mass-flux convection scheme for regional and global models. Q. J. Roy. Meteorol. Soc. 127, 869–886.

Belušić, D., Fuentes-Franco, R., Strandberg, G., Jukimenko, A., 2019. Afforestation reduces cyclone intensity and precipitation extremes over Europe. Environ. Res. Lett. 14. https://doi.org/10.1088/1748-9326/ab23b2.

Belušić, D., de Vries, H., Dobler, A., Landgren, O., Lind, P., Lindstedt, D., Pedersen, R.A., Sánchez-Perrino, J.C., Toivonen, E., van Ulft, B., Wang, F., Andrae, U., Batrak, Y., Kjellström, E., Lenderink, G., Nikulin, G., Pietikäinen, J.-P., Rodríguez-Camino, E., Samuelsson, P., van Meijgaard, E., Wu, M., 2020. HCLIM38: a flexible regional climate model applicable for different climate zones from coarse to convection-permitting scales. Geosci. Model Dev. 13, 1311–1333. https://doi.org/10.5194/gmd-13-1311-2020.

Bigler, C., Grahn, E., Larocque, I., Jeziorski, A., Hall, R., 2003. Holocene environmental change at Lake Njulla (999 m a.s.l.), northern Sweden: a comparison with four small nearby lakes along an altitudinal gradient. J. Paleolimnol. 29, 13–29. https://doi.org/10.1023/A:1022850925937.

Bigler, C., Barnekow, L., Heinrichs, M.L., Hall, R.I., 2006. Holocene environmental history of Lake Vuolop Njakajaure (Abisko National Park, northern Sweden) reconstructed using biological proxy indicators. Veget. Hist. Archaebot. 15, 309–320. https://doi.org/10.1007/s00334-006-0054-x.

Binney, H.A., Gething, P., Sugita, S., Nield, J., Edwards, M.E., 2011. Tree line identification from pollen data: beyond the limit? J. Biogeogr. 38, 1792–1806. https://doi.org/10.1111/j.1365-2699.2011.02507.x.

Bocquet-Appel, J.-P., 2011. When the world's population took off: the springboard of the neolithic demographic transition. Science 333 (6042), 560–561.

Boé, J., Somot, S., Corre, L., Nabat, P., 2020. Large discrepancies in summer climate change over Europe as projected by global and regional climate models: causes and consequences. Clim. Dynam. 54, 2981–3002. https://doi.org/10.1007/s00382-020-05153-1.

Bonferroni, C.E., 1936. Teoria statistica delle classi e calcolo delle probabilità. Pubblicazioni del R Istituto Superiore di Scienze Economiche e Commerciali di Firenze.

Borgmark, A., 2005. Holocene climate variability and periodicities in south-central Sweden interpreted from peat humification analysis. Holocene 15, 387–395. https://doi.org/10.1191/0959683605hl816rp.

Bouteloup, Y., Bouyssel, F., Marquet, P., 2005. Improvements of Lopez's progonostic large scale cloud and precipitation scheme. ALADIN Newsletter 28, 66–73.

Boysen, L.R., Brovkin, V., Pongratz, J., Lawrence, D.M., Lawrence, P., Vuichard, N., Peylin, P., Liddicoat, S., Hajima, T., Zhang, Y., Rocher, M., Delire, C., Séférian, R., Arora, V.K., Nieradzik, L., Anthoni, P., Thiery, W., Laguë, M.M., Lawrence, D., Lo, M.-H., 2020. Global climate response to idealized deforestation in CMIP6 models. Biogeosciences 17, 5615–5638. https://doi.org/10.5194/bg-17-5615-2020.

Braconnot, P., Harrison, S.P., Kageyama, M., Bartlein, P.J., Masson-Delmotte, V., Abe-Ouchi, A., Otto-Bliesner, B., Zhao, Y., 2012. Evaluation of climate models using palaeoclimatic data. Nat. Clim. Change 2, 417–424, 10.1038/nclimate1456.

Breil, M., Rechid, D., Davin, E.L., de Noblet-Ducoudré, N., Katragkou, E., Cardoso, R.M., Hoffmann, P., Jach, L.L., Soares, P.M.M., Sofiadis, G., Strada, S., Strandberg, G., Tölle, M.H., Warrach-Sagi, K., 2020. The opposing effects of re/afforestation on the diurnal temperature cycle at the surface and in the lowest atmospheric model level in the European summer. J. Clim. 33 (21), 9159–9179. https://doi.org/10.1175/JCLI-D-19-0624.1.

Brierley, C.M., Zhao, A., Harrison, S.P., Braconnot, P., Williams, C.J.R., Thornalley, D.J.R., Shi, X., Peterschmitt, J.-Y., Ohgaito, R., Kaufman, D.S., Kageyama, M., Hargreaves, J.C., Erb, M.P., Emile-Geay, J., D'Agostino, R., Chandan, D., Carré, M., Bartlein, P.J., Zheng, W., Zhang, Z., Zhang, Q., Yang, H., Volodin, E.M., Tomas, R.A., Routson, C., Peltier, W.R., Otto-Bliesner, B., Morozova, P.A., McKay, N.P., Lohmann, G., Legrande, A.N., Guo, C., Cao, J., Brady, E., Annan, J.D., Abe-Ouchi, A., 2020. Large-scale features and evaluation of the PMIP4-CMIP6 midHolocene simulations. Clim. Past 16, 1847–1872. https://doi.org/10.5194/cp-16-1847-2020.

Brooks, S., Gelman, A., Jones, G.L., Meng, X.-L., 2011. Handbook of Markov Chain Monte Carlo. CRC Press, B oca Raton, FL.

Christensen, O.B., Kjellström, E., 2020. Partitioning uncertainty components of mean climate and climate change in a large ensemble of European regional climate model projections. Clim. Dynam. 54, 4293–4308. https://doi.org/10.1007/s00382-020-05229-y.

Cuxart, J., Bougeault, P., Redelsperger, J.-L., 2000. A turbulence scheme allowing for mesoscale and large-eddy simulations. Q. J. Roy. Meteorol. Soc. 126, 1–30. https://doi.org/10.1002/qj.49712656202.

Davin, E.L., Rechid, D., Breil, M., Cardoso, R.M., Coppola, E., Hoffmann, P., Jach, L.L., Katragkou, E., de Noblet-Ducoudré, N., Radtke, K., Raffa, M., Soares, P.M.M., Sofiadis, G., Strada, S., Strandberg, G., Tölle, M.H., Warrach-Sagi, K., Wulfmeyer, V., 2020. Biogeophysical impacts of forestation in Europe: first results from the LUCAS (Land Use and Climate across Scales) regional climate model intercomparison. Earth Syst. Dyn. 11, 183–200. https://doi.org/10.5194/esd-11-183-2020.

Dawson, A., Cao, X., Chaput, M., Hopla, E., Li, F., Edwards, M., Fyfe, R., Gajewski, K., Goring, S.J., Herzschuh, U., Mazier, F., Sugita, S., Williams, J.W., Xu, Q., Gaillard, M.-J., 2018. A spatially explicit pollen-based reconstruction of

Northern Hemisphere land cover suggests open land increases of 10 to 100% across large parts of the study area over the period 6 and 0.2 ka BP. This change may have influenced past climate. Past Global Changes Magazine 26 (1), 34–35. https://doi.org/10.22498/pages.26.1.34.

Diaconu, A.-C., Tóth, M., Lamentowicz, M., Heiri, O., Kuske, E., Tanţău, I., Panait, A.-M., Braun, M., Feurdean, A., 2017. How warm? How wet? Hydroclimate reconstruction of the past 7500 years in northern Carpathians, Romania. Palaeogeogr. Palaeoclimatol. Palaeoecol. 482, 1–12. https://doi.org/10.1016/j.palaeo.2017.05.007, 2017.

Digerfeldt, G., 1998. Reconstruction and regional correlation of Holocene lake-level fluctuations in lake bysjön, south Sweden. Boreas 17, 165–182. https://doi.org/10.1111/j.1502-3885.1988.tb00544.x.

Dosio, A., Turner, A.G., Tamoffo, A.T., Sylla, M.B., Lennard, C., Jones, R.G., Terray, L., Nikulin, G., Hewitson, B., 2020. A tale of two futures: contrasting scenarios of future precipitation for West Africa from an ensemble of regional climate models. Environ. Res. Lett. 15, 064007. https://doi.org/10.1088/1748-9326/ab7fde.

Dufresne, J.L., Foujols, M.a., Denvil, S., Caubel, A., Marti, O., Aumont, O., Balkanski, Y., Bekki, S., Bellenger, H., Benshila, R., Bony, S., Bopp, L., Braconnot, P., Brockmann, P., Cadule, P., Cheruy, F., Codron, F., Cozic, A., Cugnet, D., de Noblet, N., Duvel, J.P., Ethé, C., Fairhead, L., Fichefet, T., Flavoni, S., Friedlingstein, P., Grandpeix, J.Y., Guez, L., Guilyardi, E., Hauglustaine, D., Hourdin, F., Idelkadi, A., Ghattas, J., Joussaume, S., Kageyama, M., Krinner, G., Labetoulle, S., Lahellec, A., Lefebvre, M.P., Lefevre, F., Levy, C., Li, Z.X., Lloyd, J., Lott, F., Madec, G., Mancip, M., Marchand, M., Masson, S., Meurdesoif, Y., Mignot, J., Musat, I., Parouty, S., Polcher, J., Rio, C., Schulz, M., Swingedouw, D., Szopa, S., Talandier, C., Terray, P., Viovy, N., Vuichard, N., 2013. Climate change projections using the IPSL-CM5 earth system model: from CMIP3 to CMIP5. Clim. Dynam. 40, 2123–2165. https://doi.org/10.1007/s00382-012-1636-1.

Fischer, N., Jungclaus, J.H., 2011. Evolution of the seasonal temperature cycle in a transient Holocene simulation: orbital forcing and sea-ice. Clim. Past 7, 1139–1148. https://doi.org/10.5194/cp-7-1139-2011.

Fouquart, Y., Bonnel, B., 1980. Computations of solar heating of the earth's atmosphere: a new parameterization. Beitrage zur Physik der Atmosphare 53, 35–62.

Gaillard, M.-J., Sugita, S., Mazier, F., Trondman, A.-K., Broström, A., Hickler, T., Kaplan, J.O., Kjellström, E., Kokfelt, U., Kuneš, P., Lemmen, C., Miller, P., Olofsson, J., Poska, A., Rundgren, M., Smith, B., Strandberg, G., Fyfe, R., Nielsen, A.B., Alenius, T., Balakauskas, L., Barnekow, L., Birks, H.J.B., Bjune, A., Björkman, L., Giesecke, T., Hjelle, K., Kalnina, L., Kangur, M., van der Knaap, W.O., Koff, T., Lagerås, P., Latałowa, M., Leydet, M., Lechterbeck, J., Lindbladh, M., Odgaard, B., Peglar, S., Segerström, U., von Stedingk, H., Seppä, H., 2010. Holocene land cover reconstructions for studies on land cover-climate feedbacks. Clim. Past 6, 483–499. https://doi.org/10.5194/cp-6-483-2010.

Gałka, M., Apolinarska, K., 2014. Climate change, vegetation development, and lake level fluctuations in Lake Purwin (NE Poland) during the last 8600 cal. BP based on a high-resolution plant macrofossil record and stable isotope data (δ13C and δ18O). Quat. Int. 328–329, 213–225. https://doi.org/10.1016/j.quaint.2013.12.030.

Gao, Y., Markkanen, T., Backman, L., Henttonen, H.M., Pietikäinen, J.-P., Mäkelä, H.M., Laaksonen, A., 2014. Biogeophysical impacts of peatland forestation on regional climate changes in Finland. Biogeosciences 11, 7251–7267. https://doi.org/10.5194/bg-11-7251-2014.

Garreta, V., Miller, P.A., Guiot, J., Hély, C., Brewer, S., Sykes, M.T., Litt, T., 2010. A method for climate and vegetation reconstruction through the inversion of a dynamic vegetation model. Clim. Dynam. 35, 371–389. https://doi.org/10.1007/s00382-009-0629-1.

Gilgen, A., Wilkenskjeld, S., Kaplan, J.O., Kühn, T., Lohmann, U., 2019. Effects of land use and anthropogenic aerosol emissions in the Roman Empire. Clim. Past 15, 1885–1911. https://doi.org/10.5194/cp-15-1885-2019.

Giorgi, F., 2019. Thirty years of regional climate modeling: where are we and where are we going next? J. Geophys. Res. Atmos. 124, 5696–5723. https://doi.org/10.1029/2018JD030094.

Githumbi, E., Fyfe, R., Gaillard, M.-J., Trondman, A.-K., Mazier, F., Nielsen, A.-B., Poska, A., Sugita, S., Theuerkauf, M., Woodbridge, J., Azuara, J., Feurdean, A., Grindean, R., Lebreton, V., Marquer, L., Nebout-Combourieu, N., Stancikaite, M., Tanţău, I., Tonkov, S., Shumilovskikh, L., the LandClimII Data Contributors, 2021. European pollen-based REVEALS land-cover reconstructions for the Holocene: methodology, mapping and potentials. Earth Syst. Sci. Data Discuss. https://doi.org/10.5194/essd-2021-269 [preprint].

Griscom, B.W., Adams, J., Ellis, P.W., Houghton, R.A., Lomax, G., Miteva, D.A., Schlesinger, W.H., Shoch, D., Siikamäki, J.V., Smith, P., Woodbury, P., Zganjar, C., Blackman, A., Richard, J.C., Conant, T., Delgado, C., Elias, P., Gopalakrishna, T., Hamsik, M.R., Herreso, M., Kiesecker, J., Landis, E., Laestadius, L., Leavitt, S.M., Minnemeyer, S., Polasky, S., Potapov, P., Putz, F.E., Sanderman, J., Silvius, M., Wollenberg, E., Fargione, J., 2017. Natural climate solutions. Proc. Natl. Acad. Sci. Unit. States Am. 114 (44), 11645–11650. https://doi.org/10.1073/pnas.1710465114.

Grudd, H., 2002. A 7400-year tree-ring chronology in northern Swedish Lapland: natural climatic variability expressed on annual to millenial timescales. Holocene 12, 657–665. https://doi.org/10.1191/0959683602hl578rp.

Hammarlund, D., Björck, S., Buchardt, B., Israelson, C., Thomsen, C.T., 2003. Rapid hydrological changes during the Holocene revealed by stable isotope records of lacustrine carbonates from Lake Igelsjön, southern Sweden. Quat. Sci. Rev. 22, 353–370. https://doi.org/10.1016/S0277-3791(02)00091-4.

Hammarlund, D., Velle, G., Wolfe, B.B., Edwards, T.W.D., Barnekow, L., Bergman, J., Holmgren, S., Lamme, S., Snowball, I., Wohlfarth, B., Possnert, G., 2004. Palaeolimnological responses to Holocene forest retreat in the Scandes Mountains, west-central Sweden. Holocene 14, 862–876. https://doi.org/10.1191/0959683604hl756rp.

Harrison, S., Bartlein, P., Izumi, K., Li, G., Annan, J., Hargreaves, J., Braconnot, P., Kageyama, M., 2015. Evaluation of CMIP5 palaeo-simulations to improve climate projections. Nat. Clim. Change 5, 735–743. https://doi.org/10.1038/nclimate2649.

Harrison, S.P., Bartlein, P.J., Brovkin, V., Houweling, S., Kloster, S., Prentice, I.C., 2018. The biomass burning contribution to climate-carbon cycle feedback. Earth Syst. Dynam. 9, 663–677. https://doi.org/10.5194/esd-9-663-2018.

Harrison, S.P., Gaillard, M.J., Stocker, B.D., Vander Linden, M., Klein Goldewijk, K., Boles, O., Braconnot, P., Dawson, A., Fluet-Chouinard, E., Kaplan, J.O., Kastner, T., Pausata, F.S.R., Robinson, E., Whitehouse, N.J., Madella, M., Morrison, K.D., 2020. Development and testing of scenarios for implementing Holocene LULC in earth system model experiments. Geosci. Model Dev. Discuss. (GMDD) 13 (2), 805–824. https://doi.org/10.5194/gmd-13-805-2020. ISSN 1991-962X doi:

Hazeleger, W., Severijns, C., Semmler, T., Ştefănescu, S., Yang, S., Wang, X., Wyser, K., Dutra, E., Baldasano, J.M., Bintanja, R., Bougeault, P., Caballero, R., Ekman, A.M.L., Christensen, J.H., van den Hurk, B., Jimenez, P., Jones, C., Kållberg, P., Koenigk, T., McGrath, R., Miranda, P., van Noije, T., Palmer, T., Parodi, J.A., Schmith, T., Selten, F., Storelvmo, T., Sterl, A., Tapamo, H., Vancoppenolle, M., Viterbo, P., Willén, U., 2010. EC Earth Seam. Earth Syst. Predict. Appr. Act. BAMS 91, 1357–1364. https://doi.org/10.1175/2010BAMS2877.1, 10.

He, F., Vavrus, S.J., Kutzbach, J.E., Ruddiman, W.F., Kaplan, J.O., Krumhardt, K.M., 2014. Simulating global and local surface temperature changes due to Holocene anthropogenic land cover change. Geophys. Res. Lett. 41, 623–631. https://doi.org/10.1002/2013GL058085.

Heinrichs, M.L., Peglar, S.M., Bigler, C., Birks, H.J.B., 2005. A multi-proxy palaeoecological study of Alanen Laanijärvi, a boreal-forest lake in Swedish Lapland. Boreas 34, 192–206. https://doi.org/10.1111/j.1502-3885.2005.tb01015.x.

Heinrichs, M., Barnekow, L., Rosenberg, S.A., 2006. Comparison of chironomid biostratigraphy from Lake Vuolep Njakajaure with vegetation, lake-level, and climate changes in Abisko National Park, Sweden. J. Paleolimnol. 36, 119–131. https://doi.org/10.1007/s10933-006-0010-x.

Heiri, O., Lotter, A.F., 2005. Holocene and Lateglacial summer temperature reconstruction in the Swiss Alps based on fossil assemblages of aquatic organisms: a review. Boreas 34, 506–516. https://doi.org/10.1080/03009480500231229.

Helama, S., Lindholm, M., Timonen, M., Meriläinen, J., Eronen, M., 2002. The supralong Scots pine tree-ring record for Finnish Lapland. Part 2: interannual to centennial variability in summer temperatures for 7500 years. Holocene 12, 681–687. https://doi.org/10.1191/0959683602hl581rp.

Hickler, T., Vohland, K., Feehan, J., Miller, P.A., Smith, B., Costa, L., Giesecke, T., Fronzek, S., Carter, T.R., Cramer, W., Kühn, I., Sykes, M.T., 2012. Projecting the future distribution of European potential natural vegetation zones with a generalized, tree species-based dynamic vegetation model. Global Ecol. Biogeogr. 21, 50–63. https://doi.org/10.1111/j.1466-8238.2010.00613.x.

Hughes, P.D.M., Barber, K.E., Langdon, P.G., Mauquoy, D., 2000. Mire-development pathways and palaeoclimatic records from a full Holocene peat archive at Walton Moss, Cumbria, England. Holocene 10, 465–479. https://doi.org/10.1191/095968300675142023.

Iacono, M.J., Delamere, J.S., Mlawer, E.J., Shephard, M.W., Clough, S.A., Collins, W.D., 2008. Radiative forcing by longlived greenhouse gases: calculations with the AER radiative transfer models. J. Geophys. Res. Atmos. 113, D13103. https://doi.org/10.1029/2008JD009944.

Ikonen, L., 1993. Holocene development and peat growth of the raised bog Pesänsuo in southwestern Finland. In: Bulletin, vol. 370. Geological Survey of Finland, Espoo, 1993.

IPCC, 2018. Summary for Policymakers Global Warming of 1.5°C. An IPCC Special Report on the impacts of global warming of 1.5°C above pre-industrial levels and related global greenhouse gas emission pathways. In: Zhai, P., Pörtner, H.-O., Roberts, D., Skea, J., Shukla, P.R., Pirani, A., Moufouma-Okia, W., Péan, C., Pidcock, R., Connors, S., Matthews, J.B.R., Chen, Y., Zhou, X., Gomis, M.I., Lonnoy, E., Maycock, T., Tignor, M., Waterfield, T. (Eds.), The Context of Strengthening the Global Response to the Threat of Climate Change, Sustainable Development, and Efforts to Eradicate Poverty [Masson-Delmotte, V. Press.

Jacob, D., Petersen, J., Eggert, B., Alias, A., Christensen, O.B., Bouwer, L.M., Braun, A., Colette, A., Déqué, M., Georgievski, G., Georgopoulou, E., Gobiet, A., Menut, L., Nikulin, G., Haensler, A., Hempelmann, N., Jones, C., Keuler, K., Kovats, S., Kröner, N., Kotlarski, S., Kriegsmann, A., Martin, E., van Meijgaard, E., Moseley, C., Pfeifer, S., Preuschmann, S., Radermacher, C., Radtke, K., Rechid, D., Rounsevell, M., Samuelsson, P., Somot, S., Soussana, J.-F., Teichmann, C., Valentini, R., Vautard, R., Weber, B., Yiou, P., 2014. EURO-CORDEX: new high-resolution climate change projections for European impact research. Reg. Environ. Change 14 (2), 563–578. 10.1007/s10113-013-0499-2.

Jerez, S., López-Romero, J.M., Turco, M., et al., 2018. Impact of evolving greenhouse gas forcing on the warming signal in regional climate model experiments. Nat. Commun. 9, 1304. https://doi.org/10.1038/s41467-018-03527-y.

Jia, G., Shevliakova, E., Artaxo, P., De Noblet-Ducoudré, N., Houghton, R., House, J., Kitajima, K., Lennard, C., Popp, A., Sirin, A., Sukumar, R., Verchot, L., 2019. Land–climate interactions. In: Shukla, P.R., Skea, J., Calvo Buendia, E., Masson-Delmotte, V., Pörtner, H.-O., Roberts, D.C., Zhai, P., Slade, R., Connors, S., van Diemen, R., Ferrat, M., Haughey, E., Luz, S., Neogi, S., Pathak, M., Petzold, J., Portugal Pereira, J., Vyas, P., Huntley, E., Kissick, K., Belkacemi, M., Malley, J.

(Eds.), Climate Change and Land: an IPCC Special Report on Climate Change, Desertification, Land Degradation, Sustainable Land Management, Food Security, and Greenhouse Gas Fluxes in Terrestrial Ecosystems (in press).
Kageyama, M., Braconnot, P., Harrison, S.P., Haywood, A.M., Jungclaus, J.H., Otto-Bliesner, B.L., Peterschmitt, J.-Y., AbeOuchi, A., Albani, S., Bartlein, P.J., Brierley, C., Crucifix, M., Dolan, A., Fernandez-Donado, L., Fischer, H., Hopcroft, P.O., Ivanovic, R.F., Lambert, F., Lunt, D.J., Mahowald, N.M., Peltier, W.R., Phipps, S.J., Roche, D.M., Schmidt, G.A., Tarasov, L., Valdes, P.J., Zhang, Q., Zhou, T., 2018. The PMIP4 contribution to CMIP6 – Part 1: overview and overarching analysis plan. Geosci. Model Dev. 11, 1033–1057. https://doi.org/10.5194/gmd-11-1033-2018.
Kaplan, J.O., Krumhardt, K.M., 2011. The KK10 Anthropogenic Land Cover Change Scenario for the Preindustrial Holocene, Link to Data in NetCDF Format. PANGAEA. https://doi.org/10.1594/PANGAEA.871369.
Kaplan, J., Krumhardt, K., Zimmermann, N., 2009. The prehistoric and preindustrial deforestation of Europe. Quat. Sci. Rev. 28, 3016–3034. https://doi.org/10.1016/j.quascirev.2009.09.028.
Kaplan, J.O., Krumhardt, K.M., Ellis, E.C., Ruddiman, W.F., Lemmen, C., Goldewijk, K.K., 2010. Holocene carbon emissions as a result of anthropogenic land cover change. Holocene 1–17. https://doi.org/10.1177/0959683610386983.
Kaplan, J.O., Krumhardt, K.M., Gaillard, M.-J., Sugita, S., Trondman, A.-K., Fyfe, R., Marquer, L., Mazier, F., Nielsen, A.B., 2017. Constraining the deforestation history of Europe: evaluation of historical land use scenarios with pollen-based land cover reconstructions. Land 6, 91. https://doi.org/10.3390/land6040091.
Kjellström, E., Brandefelt, J., Näslund, J.-O., Smith, B., Strandberg, G., Voelker, A.H.L., Wohlfarth, B., 2010. Simulated climate conditions in Europe during the marine isotope stage 3 stadial. Boreas. https://doi.org/10.1111/j.1502-3885.2010.00143.x.ISSN0300-9483.
Kjellström, E., Bärring, L., Nikulin, G., Nilsson, C., Persson, N., Strandberg, G., 2016. Production and use of regional climate model projections – a Swedish perspective on building climate services. Clim. Serv. 2–3, 15–29. https://doi.org/10.1016/j.cliser.2016.06.004.
Kjellström, E., Nikulin, G., Strandberg, G., Christensen, O.B., Jacob, D., Keuler, K., Lenderink, G., van Meijgaard, E., Schär, C., Somot, S., Sørland, S.L., Teichmann, C., Vautard, R., 2018. European climate change at global mean temperature increases of 1.5 and 2 °C above pre-industrial conditions as simulated by the EURO-CORDEX regional climate models. Earth Syst. Dynam. 9, 459–478. https://doi.org/10.5194/esd-9-459-2018.
Klein Goldewijk, K., Beusen, A., de Vos, M., van Drecht, G., 2011. The HYDE 3.1 spatially explicit database of human induced land use change over the past 12,000 years. Global Ecol. Biogeogr. 20, 73–86. https://doi.org/10.1111/j.1466-8238.2010.00587.x.
Korhola, A., Weckström, J., Holmström, L., Erästö, P., 2000. A quantitative Holocene climatic record from diatoms in northern Fennoscandia. Quat. Res. (Duluth) 54, 284–294. https://doi.org/10.1006/qres.2000.2153.
Larocque-Tobler, I., Heiri, O., Wehrli, M., 2010. Late Glacial and Holocene temperature changes at Egelsee, Switzerland, reconstructed using subfossil chironomids. J. Paleolimnol. 43, 649–666. https://doi.org/10.1007/s10933-009-9358-z.
Laroque, I., Hall, R.I., 2004. Holocene temperature estimates and chironomid community composition in the Abisko valley, northern Sweden. Quat. Sci. Rev. 23, 2453–2465. https://doi.org/10.1016/j.quascirev.2004.04.006.
Li, L., Pengfei Lin, P., Yu, Y., Wang, B., Zhou, T., Liu, L., Liu, J., Bao, Q., Xu, S., Huang, W., Xia, K., Pu, Y., Dong, L., Shen, S., Liu, Y., Hu, N., Liu, M., Sun, W., Shi, X., Zheng, W., Wu, B., Song, M., Liu, H., Zhang, X., Wu, G., Xue, W., Huang, X., Yang, G., Song, Z., Qiao, F., 2013. The flexible global ocean–atmosphere–land system model, Grid-point Version 2: FGOALS-g2. Adv. Atmos. Sci. 30 (19), 543–560. https://doi.org/10.1007/s00376-012-2140-6.
Lind, P., Belušić, D., Christensen, O.B., Dobler, A., Kjellström, E., Landgren, O., Lindstedt, D., Matte, D., Pedersen, R.A., Toivonen, E., Wang, F., 2020. Benefits and added value of convection-permitting climate modeling over Fenno-Scandinavia. Clim. Dynam. https://doi.org/10.1007/s00382-020-05359-3.
Lindgren, F., Rue, H., Lindström, J., 2011. An explicit link between Gaussian fields and Gaussian Markov random fields: the stochastic partial differential equation approach. J. Roy. Stat. Soc. B Stat. Methodol. 73 (4), 423–498. https://doi.org/10.1111/j.1467-9868.2011.00777.x.
Liu, Z., Zhu, J., Rosenthal, Y., Zhang, X., Otto-Bliesner, B.L., Timmermann, A., Smith, R.S., Lohmann, G., Zheng, W., Elison, T.O., 2014. The Holocene temperature conundrum. Proc. Natl. Acad. Sci. Unit. States Am. https://doi.org/10.1073/pnas.1407229111. E3501-E3505, 111, 34.
Lopez, P., 2002. Implementation and validation of a new prognostic large-scale cloud and precipitation scheme for climate and dataassimilation purposes. Q. J. Roy. Meteorol. Soc. 128, 229–257. https://doi.org/10.1256/00359000260498879.
Lu, Z., Miller, P.A., Zhang, Q., Zhang, Q., Wårlind, D., Nieradzik, L., Sjolte, J., Smith, B., 2018. Dynamic vegetation simulations of the mid-holocene green Sahara. Geophys. Res. Lett. 45, 8294–8303. https://doi.org/10.1029/2018GL079195.
Ludwig, P., Gómez-Navarro, J. J., Pinto, J. G., Raible, C. C., Wagner, S., and Zorita, E., 2019 Perspectives of regional paleoclimate modeling, Ann. NY. Acad. Sci., 1436, 54-69, https://doi.org/10.1111/nyas.13865.
Ludwig, P., Shao, Y., Kehl, M., Weniger, G.-C., 2018. The Last Glacial Maximum and Heinrich event I on the Iberian Peninsula: a regional climate modelling study for understanding human settlement patterns. Global Planet. Change 170, 34–47. https://doi.org/10.1016/j.gloplacha.2018.08.006.
Luoto, P.T., Kultti, S., Nevalainen, L., Sarmaja-Korjonen, K., 2010. Temperature and effective moisture variability in southern Finland during the Holocene quantified with midge-based calibration models. J. Quat. Sci. 25, 1317–1326. ISSN 0267-8179.
Magny, M., 2004. Holocene climate variability as reflected by mid-European lake-level fluctuations and its probable impact on pre-historic human settlements. Quat. Int. 113, 65–79. https://doi.org/10.1016/S1040-6182(03)00080-6.
Marcott, S.A., Shakun, J.D., Clark, P.U., Mix, A.C., 2013. A reconstruction of regional and global temperature for the past 11,300 years. Science 339, 1198–1201. https://doi.org/10.1126/science.1228026.
Masson, V., Le Moigne, P., Martin, E., Faroux, S., Alias, A., Alkama, R., Belamari, S., Barbu, A., Boone, A., Bouyssel, F., Brousseau, P., Brun, E., Calvet, J.-C., Carrer, D., Decharme, B., Delire, C., Donier, S., Essaouini, K., Gibelin, A.-L., Giordani, H., Habets, F., Jidane, M., Kerdraon, G., Kourzeneva, E., Lafaysse, M., Lafont, S., Lebeaupin Brossier, C., Lemonsu, A., Mahfouf, J.-F., Marguinaud, P., Mokhtari, M., Morin, S., Pigeon, G., Salgado, R., Seity, Y., Taillefer, F., Tanguy, G., Tulet, P., Vincendon, B., Vionnet, V., Voldoire, A., 2013. The SURFEXv7.2 land and ocean surface platform for coupled or offline simulation of earth surface variables and fluxes. Geosci. Model Dev. 6, 929–960. https://doi.org/10.5194/gmd-6-929-2013.
Mauri, A., Davis, B.A.S., Collins, P.M., Kaplan, J.O., 2014. The influence of atmospheric circulation on the mid-Holocene climate of Europe: a data–model comparison. Clim. Past 10, 1925–1938. https://doi.org/10.5194/cp-10-1925-2014.
Mazier, F., Gaillard, M.-J., Kuneš, P., Sugita, S., Trondman, A.-K., Broström, A., 2012. Testing the effect of site selection and parameter setting on REVEALS-model estimates of plant abundance using the Czech Quaternary Palynological Database. Rev. Palaeobot. Palynol. 187, 38–49. https://doi.org/10.1016/j.revpalbo.2012.07.017.
Miller, P.A., Giesecke, T., Hickler, T., Bradshaw, R.H.W., Smith, B., Seppä, H., Valdes, P.J., Sykes, M.T., 2008. Exploring climatic and biotic controls on Holocene vegetation change in Fennoscandia. J. Ecol. 96, 247–259. https://doi.org/10.1111/j.1365-2745.2007.01342.x.
Mlawer, E.J., Taubman, S.J., Brown, P.D., Iacono, M.J., Clough, S.A., 1997. Radiative transfer for inhomogeneous atmospheres: RRTM, a validated correlated-k model for the longwave. J. Geophys. Res. Atmos. 102, 16663–16682. https://doi.org/10.1029/97JD00237.
Monsi, M., Saeki, T., 1953. Über den Lichtfaktor in den Pflanzengesellschaften und seine Bedeutung für die Stoffproduktion. Jpn. J. Bot. 14, 22–52.
Muschitiello, F., Zhang, Q., Sundqvist, H.S., Davies, F.J., Renssen, H., 2015. Arctic climate response to the termination of the african humid period. Quat. Sci. Rev. 125, 91–97.
Niggeman, S., Mangini, A., Richter, D.K., Wurth, G., 2003. A paleo-climate record of the last 17.600 years from the B7 cave, Sauerland, Germany. Quat. Sci. Rev. 22, 555–567. https://doi.org/10.1016/S0277-3791(02)00143-9.
Olsen, J., Noe-Nygaard, N., Wolfe, B.B., 2010. Mid to Late Holocene climate variability and anthropogenic impacts; multi-proxy evidence from lake Bliden, Denmark. J. Paleolimnol. 43, 323–343. https://doi.org/10.1007/s10933-009-9334-7.
Otto-Bliesner, B.L., Braconnot, P., Harrison, S.P., Lunt, D.J., Abe-Ouchi, A., Albani, S., Bartlein, P.J., Capron, E., Carlson, A.E., Dutton, A., Fischer, H., Goelzer, H., Govin, A., Haywood, A., Joos, F., LeGrande, A.N., Lipscomb, W.H., Lohmann, G., Mahowald, N., Nehrbass-Ahles, C., Pausata, F.S.R., Peterschmitt, J.Y., Phipps, S.J., Renssen, H., Zhang, Q., 2017. The PMIP4 contribution to CMIP6 – Part 2: two interglacials, scientific objective and experimental design for Holocene and Last Interglacial simulations. Geosci. Model Dev. 10, 3979–4003. https://doi.org/10.5194/gmd-10-3979-2017.
Pausata, F.S.R., Messori, G., Zhang, Q., 2016. Impacts of dust reduction on the northward expansion of the African monsoon during the Green Sahara period. Earth Planet Sci. Lett. 434, 298–307. https://doi.org/10.1016/j.epsl.2015.11.049.
Perşoiu, A., Onac, B.P., Wynn, J.G., Blaauw, M., Ionita, M., Hansson, M., 2017. Holocene winter climate variability in central and eastern Europe. Sci. Rep. 7, 1196. https://doi.org/10.1038/s41598-017-01397-w.
Peyron, O., Combourieu-Nebout, N., Brayshaw, D., Goring, S., Andrieu-Ponel, V., Desprat, S., Fletcher, W., Gambin, B., Ioakim, C., Joannin, S., Kotthoff, U., Kouli, K., Montade, V., Pross, J., Sadori, L., Magny, M., 2017. Precipitation changes in the Mediterranean basin during the Holocene from terrestrial and marine pollen records: a model–data comparison. Clim. Past 13, 249–265. https://doi.org/10.5194/cp-13-249-2017.
Pirzamanbein, B., Lindström, J., Poska, A., Gaillard, M.-J., 2018. Modelling spatial compositional data: reconstructions of past land cover and uncertainties. Spat. Stat. 24, 14–31. https://doi.org/10.1016/j.spasta.2018.03.005. April 2018.
Pirzamanbein, B., Poska, A., Lindström, J., 2020. Bayesian reconstruction of past land cover from pollen data: model robustness and sensitivity to auxiliary variables. Earth Space Sci. 7, 1. https://doi.org/10.1029/2018EA000547.
Prentice, I.C., Sykes, M.T., Cramer, W., 1993. A simulation model for the transient effects of climate change on forest landscapes. Ecol. Model. 65, 51–70. https://doi.org/10.1016/0304-3800(93)90126-D.
Rana, A., Nikulin, G., Kjellström, E., Strandberg, G., Kupiainen, M., Hansson, U., Kolax, M., 2020. Contrasting regional and global climate simulations over South Asia. Clim. Dynam. 54, 2883–2901. https://doi.org/10.1007/s00382-020-05146-0.
Renssen, H., Seppä, H., Heiri, O., Roche, D.M., Goosse, H., Fichefet, T., 2009. The spatial and temporal complexity of the Holocene thermal maximum. Nat. Geosci. 2, 411–414. https://doi.org/10.1038/ngeo513.
Ritchie, H., Temperton, C., Simmons, A., Hortal, M., Davies, T., Dent, D., Hamrud, M., 1995. Implementation of the semi-Lagrangian method in a HighResolution version of the ECMWF forecast model. Mon. Weather Rev. 123, 489–514. https://doi.org/10.1175/1520- 0493(1995)123<0489:IOTSLM>2.0.CO;2.
Robert, A.J., Henderson, J., Turnbull, C., 1972. An implicit scheme for baroclinic

models of the atmosphere. Mon. Weather Rev. 100, 329–335.
Roberts, G.O., Stramer, O., 2002. Langevin diffusions and metropolis-hastings algorithms. Methodol. Comput. Appl. Probab. 4, 337–357. https://doi.org/10.1023/A:1023562417138.
Rosén, P., Segerström, U., Eriksson, L., Renberg, I., Birks, H.J.B., 2001. Holocene climatic change reconstructed from diatoms, chironomids, pollen and near-infrared spectroscopy at an alpine lake (Sjuodjijaure) in northern Sweden. Holocene 11, 551–562. https://doi.org/10.1191/095968301680223503.
Rotstayn, L.D., Jeffrey, S.J., Collier, M.A., Dravitzki, S.M., Hirst, A.C., Syktus, J.I., Wong, K.K., 2012. Aerosol-and greenhouse gas-induced changes in summer rainfall andcirculation in the Australasian region: a study using single-forcing climate simulations. Atmos. Chem. Phys. 12, 6377–6404. https://doi.org/10.5194/acp-12-6377-2012.
Ruddiman, W.F., Ellis, E.C., Kaplan, J.O., Fuller, D.Q., 2015. Defining the epoch we live in. Science 348 (6230), 38–39. https://doi.org/10.1126/science.aaa7297, 03.
Rummukainen, M., 2016. Added value in regional climate modeling. Wire Clim. Change 7, 145–159. https://doi.org/10.1002/wcc.378, 2016.
Russo, E., Cubasch, U., 2016. Mid-to-late Holocene temperature evolution and atmospheric dynamics over Europe in regional model simulations. Clim. Past 12, 1645–1662. https://doi.org/10.5194/cp-12-1645-2016.
Russo, E., Fallah, B., Ludwig, P., Karremann, M., Raible, C.C., 2021. The long-standing dilemma of European summer temperatures at the Mid-Holocene and other considerations on learning from the past for the future using a regional climate model [preprint] Clim. Past Discuss. https://doi.org/10.5194/cp-2021-101 (submitted for publication).
Schimanke, S., Meier, H.E.M., Kjellström, E., Strandberg, G., Hordoir, R., 2012. The climate in the Baltic Sea region during the last millennium simulated with a regional climate model. Clim. Past 8, 1419–1433. https://doi.org/10.5194/cp-8-1419-2012.
Schmidt, G.A., Kelley, M., Nazarenko, L., Ruedy, R., Russell, G.L., Aleinov, I., Bauer, M., Bauer, S.E., Bhat, M.K., Bleck, R., Canuto, 25V., Chen, Y.-h., Cheng, Y., Clune, T.L., Genio, A.D., Fainchtein, R.D., Faluvegi, G., Hansen, J.E., Healy, R.J., Kiang, N.Y., Koch, D., Lacis, A.a., Legrande, A.N., Lerner, J., Lo, K.K., Matthews, E.E., Menon, S., Miller, R.L., Oinas, V., Oloso, A.O., Perlwitz, J.P., Puma, M.J., Putman, W.M., Rund, D., Romanou, A., Sato, M., Shindell, D.T., Sun, S., Syed, R.A., Tausnev, N., Tsigaridis, K., Unger, N., Voulgarakis, A., Yao, M.-S., Zhang, J., 2014. Configuration and assessment of the GISS ModelE2 contributions to the CMIP5 archive. J. Adv. Model. Earth Syst. 6, 141–184. https://doi.org/10.1002/2013MS000265.
Simmons, A.J., Hoskins, B., Burridge, D., 1978. Stability of the semiimplicit method of time integration. Mon. Weather Rev. 106, 405–412.
Sitch, S., Smith, B., Prentice, I.C., Arneth, A., Bondeau, A., Cramer, W., Kaplan, J.O., Levis, S., Lucht, W., Sykes, M.T., Thonicke, K., Vevensky, S., 2003. Evaluation of ecosystem dynamics, plant geography and terrestrial carbon cycling in the LPJ dynamic global vegetation model. Global Change Biol. 9, 161–185. https://doi.org/10.1046/j.1365-2486.2003.00569.x.
Smith, B., Prentice, I.C., Sykes, M.T., 2001. Representation of vegetation dynamics in the modelling of terrestrial ecosystems: comparing two contrasting approaches within European climate space. Global Ecol. Biogeogr. 10, 621–637. https://doi.org/10.1046/j.1466-822X.2001.t01-1-00256.x.
Smith, B., Wårlind, D., Arneth, A., Hickler, T., Leadley, P., Siltberg, J., Zaehle, S., 2014. Implications of incorporating N cycling and N limitations on primary production in an individual-based dynamic vegetation model. Biogeosciences 11, 2027–2054. https://doi.org/10.5194/bg-11-2027-2014.
Smith, P., Davis, S., Creutzig, F., et al., 2016a. Biophysical and economic limits to negative CO2 emissions. Nat. Clim. Change 6, 42–50. https://doi.org/10.1038/nclimate2870.
Smith, M.C., Singarayer, J.S., Valdes, P.J., Kaplan, J.O., Branch, N.P., 2016b. The biogeophysical climatic impacts of anthropogenic land use change during the Holocene. Clim. Past 12, 923–941. https://doi.org/10.5194/cp-12-923-2016.
Snowball, I., Sandgren, P., 1996. Lake sediment studies of Holocene glacial activity, northern Sweden: contrasts in interpretation. Holocene 6, 367–372. https://doi.org/10.1177/095968369600600312.
Sørland, S.L., Schär, C., Lüthi, D., Kjellström, E., 2018. Bias patterns and climate change signals in GCM-RCM model chains. Environ. Res. Lett. 13, 074017. https://doi.org/10.1088/1748-9326/aacc7.
Stadelmaier, K.H., Ludwig, P., Bertran, P., Antoine, P., Shi, X., Lohmann, G., Pinto, J.G., 2021. A new perspective on permafrost boundaries in France during the Last Glacial Maximum, Clim. Past 17, 2559–2576. https://doi.org/10.5194/cp-17-2559-2021.
Stevens, B., Giorgetta, M., Esch, M., Mauritsen, T., Crueger, T., Rast, S., Salzmann, M., Schmidt, H., Bader, J., Block, K., Brokopf, R., Fast, I., Kinne, S., Kornblueh, L., Lohmann, U., Pincus, R., Reichler, T., Roeckner, E., 2013. The atmospheric component of the MPI-M earthsystem model: ECHAM6. J. Adv. Model. Earth Syst. 5, 1–27. https://doi.org/10.1002/jame.20015 http://doi.wiley.com/10.1002/jame.20015-2013.
Stocker, B.D., Yu, Z., Massa, C., Joos, F., 2017. Holocene peatland and ice-core data constraints on the timing and magnitude of CO2 emissions from past land use. P. Natl. Acad. Sci. USA 114, 1492–1497. https://doi.org/10.1073/pnas.1613889114.
Strandberg, G., Kjellström, E., 2019. Climate impacts from afforestation and deforestation in Europe. Earth Interact. 23, 1–27. https://doi.org/10.1175/EI-D-17-0033.1.
Strandberg, G., Lind, P., 2021. The importance of horizontal model resolution on simulated precipitation. Weather Clim. Dynam. 2, 181–204. https://doi.org/10.5194/wcd-2-181-2021.
Strandberg, G., Brandefelt, J., Kjellström, E., Smith, B., 2011. High-resolution regional simulation of last glacial maximum climate over Europe. Tellus 63A, 107–125. https://doi.org/10.1111/j.1600-0870.2010.00485.x.
Strandberg, G., Kjellström, E., Poska, A., Wagner, S., Gaillard, M.-J., Trondman, A.-K., Mauri, A., Davis, B.A.S., Kaplan, J.O., Birks, H.J.B., Bjune, A.E., Fyfe, R., Giesecke, T., Kalnina, L., Kangur, M., van der Knaap, W.O., Kokfelt, U., Kuneš, P., Latalowa, M., Marquer, L., Mazier, F., Nielsen, A.B., Smith, B., Seppä, H., Sugita, S., 2014. Regional climate model simulations for Europe at 6 and 0.2 k BP: sensitivity to changes in anthropogenic deforestation. Clim. Past 10, 661–680. https://doi.org/10.5194/cp-10-661-2014.
Strandberg, G., Bärring, L., Hansson, U., Jansson, C., Jones, C., Kjellström, E., Kolax, M., Kupiainen, M., Nikulin, G., Samuelsson, P., Ullerstig, A., Wang, S., 2015. CORDEX scenarios for Europe from the Rossby Centre regional climate model RCA4. SMHI Meteorol. Climatol. Rep. 116, 84. Norrköping. https://www.smhi.se/polopoly_fs/1.90275!/Menu/general/extGroup/attachmentColHold/mainCol1/file/RMK_116.pdf.
Sugita, S., 2007. Theory of quantitative reconstruction of vegetation I: pollen from large sites REVEALS regional vegetation composition. Holocene 17 (2), 229–241. https://doi.org/10.1177/0959683607075837.
Temperton, C., Hortal, M., Simmons, A., 2001. A two-time-level semi-Lagrangian global spectral model. Q. J. Roy. Meteorol. Soc. 127, 111–127.
Trondman, A.-K., Gaillard, M.-J., Mazier, F., Sugita, S., Fyfe, R.M., Nielsen, A.B., Twiddle, C., Barratt, P., Birks, H.J.B., Bjune, A.E., Björkman, L., Broström, A., Caseldine, C.J., David, R., Dodson, J., Dörfler, W., Fischer, E., van Geel, B., Giesecke, T., Hultberg, T., Kalnina, L., Kangur, M., van der Knaap, P.W.O., Koff, T., Kunes, P., Lageras, P., Latalowa, M., Lechterbeck, J., Leroyer, C., Leydet, M., Lindbladh, M., Marquer, L., Mitchell, F.J.G., Odgaard, B.V., Peglar, S.M., Persson, T., Poska, A., Rösch, M., Seppä, H., Veski, S., Wick, L., 2015. Pollen-based quantitative reconstructions of Holocene regional vegetation cover (plant-functional types and land-cover types) in Europe suitable for climate modelling. Global Change Biol. 21 (2), 676–697. https://doi.org/10.1111/gcb.12737.
Trondman, A.-K., Gaillard, M.-J., Sugita, S., Björkman, L., Greisman, A., Hultberg, T., Lagerås, P., Lindbladh, M., Mazier, F., 2016. Are pollen records from small sites appropriate for REVEALS model-based quantitative reconstructions of past regional vegetation? An empirical test in southern Sweden. Veg. Hist. Archaeobotany 25, 131–151. https://doi.org/10.1007/s00334-015-0536-9.
UNFCCC, 2015. The Paris Agreement. United Nations Framework Convention on Climate Change. http://unfccc.int/paris_agreement/items/9485.php. (Accessed 1 July 2021). accessed.
UNFCCC, 2010. The cancun agreements. United nations framework convention on climate change. accessed 1 July 2021. http://unfccc.int/meetings/cancunnov2010/meeting/6266.php.
Valcke, S., 2013. The OASIS3 coupler: a European climate modelling community software, Geosci. Model Dev 6, 373–388. https://doi.org/10.5194/gmd-6-373-2013.
Vancoppenolle, M., Fichefet, T., Goosse, H., Bouillon, S., Madec, G., Maqueda, M.A.M., 2009. Simulating the mass balance and salinity of arctic and antarctic sea ice. Ocean Model. 27, 33–53. https://doi.org/10.1016/j.ocemod.2008.10.005.
Vautard, R., Kadygrov, N., Iles, C., Boberg, F., Buonomo, E., Bülow, K., Coppola, E., Corre, L., Meijgaard, E., Nogherotto, R., Sandstad, M., Schwingshackl, C., Somot, S., Aalbers, E., Christensen, O.B., Ciarlò, J.M., Demory, M.-E., Giorgi, F., Jacob, D., Jones, R.G., Keuler, K., Kjellström, E., Lenderink, G., Levavasseur, G., Nikulin, G., Sillmann, J., Solidoro, C., Sørland, S.L., Steger, C., Teichmann, C., Warrach-Sagi, K., Wulfmeyer, V., 2020. Evaluation of the large EURO-CORDEX regional climate model ensemble. J. Geophys. Res. Atmos. 125, e2019JD032344. https://doi.org/10.1029/2019JD032344, 2020.
Velasquez, P., Kaplan, J.O., Messmer, M., Ludwig, P., Raible, C.C., 2021. The role of land cover in the climate of glacial Europe. Clim. Past 17, 1161–1180. https://doi.org/10.5194/cp-17-1161-2021.
Velle, G., Brooks, S.J., Birks, H.J.B., Willassen, E., 2005. Chironomids as a tool for inferring Holocene climate: an assessment based on six sites in southern Scandinavia. Quat. Sci. Rev. 24, 1429–1462. https://doi.org/10.1016/j.quascirev.2004.10.010.
Voldoire, A., Sánchez-Gómez, E., Salas y Mélia, D., Decharme, B., Cassou, C., Sénési, S., Valcke, S., Beau, I., Alias, A., Chevallier, M., Déqué, M., Deshayes, J., Douville, H., Fernandez, E., Madec, G., Maisonnave, E., Moine, M.-P., Planton, S., Saint-Martin, D., Szopa, S., Tyteca, S., Alkama, R., Belamari, S., Braun, A., Coquart, L., Chauvin, F., 2012. The CNRM-CM5.1 global climate model: description and basic evaluation. Clim. Dynam. 40, 2091–2121. https://doi.org/10.1007/s00382-011-1259-y.
Walczak, I.W., et al., 2015. Reconstructing high-resolution climate using CT scanning of unsectioned stalagmites: a case study identifying the mid-Holocene onset of the Mediterranean climate in southern Iberia. Quat. Sci. Rev. https://doi.org/10.1016/j.quascirev.2015.06.013.
Wanner, H., Beer, J., Bütikofer, J., Crowley, T.J., Cubasch, U., Flückiger, J., Goosse, H., Grosjean, M., Joos, F., Kaplan, J.O., Küttel, M., Müller, S.A., Prentice, I.C., Solomina, O., Stocker, T.F., Tarasov, P., Wagner, M., Widmann, M., 2008. Mid- to late Holocene climate change: an overview. Quat. Sci. Rev. 27, 1791–1828. https://doi.org/10.1016/j.quascirev.2008.06.013.
Watanabe, S., Hajima, T., Sudo, K., Nagashima, T., Takemura, T., Okajima, H., Nozawa, T., Kawase, H., Abe, M., Yokohata, T., Ise, T., Sato, H., Kato, E., Takata, K., Emori, S., Kawamiya, M., 2011. MIROC-ESM 2010: model description and basic results ofCMIP5-20c3m experiments, Geosci. Model Dev 4, 845–872. https://doi.org/10.5194/gmd-4-845-2011.
Williamson, P., 2016. Scrutinize CO2 removal methods. Nature 530, 153–155. https://doi.org/10.1038/530153a.

Wu, T., Song, L., Li, W., Wang, Z., Zhang, H., Xin, X., Zhang, Y., Zhang, L., Li, J., Wu, F., Liu, Y., Zhang, F., Shi, X., Chu, M., Zhang, J., Fang, Y., Wang, F., Lu, Y., Liu, X., Wei, M., Liu, Q., Zhou, W., Dong, M., Zhao, Q., Ji, J., Li, L., Zhou, M., 2014. An overview of BCCclimate system model development and application for climate change studies. J. Meteorol. Res. 28, 34–56. https://doi.org/10.1007/s13351-014-3041-7.

Xu, C., Yan, M., Ning, L., Liu, J., 2020. Summer westerly jet in northern hemisphere during the mid-holocene: a multi-model study. Atmosphere 11 (11), 1193. https://doi.org/10.3390/atmos11111193.

Yukimoto, S., Adachi, Y., Hosaka, M., Sakami, T., Yoshimura, H., Hirabara, M., Tanaka, T.Y., Shindo, E., Tsujino, H., Deushi, M., Mizuta, R., Yabu, S., Obata, A., Nakano, H., Koshiro, T., Ose, T., Kitoh, A., 2012. A new global climate model of the mete-orological research institute: MRI-CGCM3—Model descriptionand basic performance. J. Meteorol. Soc. Jpn., Ser. II 90A, 23–64. https://doi.org/10.2151/jmsj.2012-A02.

Zhang, Q., Berntell, E., Axelsson, J., Chen, J., Han, Z., de Nooijer, W., Lu, Z., Li, Q., Zhang, Q., Wyser, K., Yang, S., 2021. Simulating the mid-Holocene, last interglacial and mid-Pliocene climate with EC-Earth3-LR, Geosci. Model Dev 14, 1147–1169. https://doi.org/10.5194/gmd-14-1147-2021.